Radiolarian response to environmental changes at the Sinemurian–Pliensbachian transition in the Northern Calcareous Alps, Austria

by TIM CIFER[1],* (iD), ŠPELA GORIČAN[1] (iD), ATTILA DEMÉNY[2] (iD) *and* HANS-JÜRGEN GAWLICK[3] (iD)

[1]Ivan Rakovec Institute of Palaeontology, Research Centre of the Slovenian Academy of Sciences & Arts, Novi trg 2, Ljubljana SI-1000, Slovenia; tim.cifer@zrc-sazu.si, spela.gorican@zrc-sazu.si

[2]Institute for Geological & Geochemical Research, Research Centre for Astronomy & Earth Sciences, Budaorsi ut 45, Budapest H-1112, Hungary; demeny.attila@csfk.org

[3]Montanuniversität Leoben, Department of Petroleum Geology, Peter-Tunner-Straße 5, 8700 Leoben, Austria; hans-juergen.gawlick@unileoben.ac.at

*Corresponding author

Abstract: Major environmental, climate and sealevel changes occurred in the Western Tethyan Realm during the late Sinemurian to early Pliensbachian time interval. Here, we examine how these changes affected the taxonomic composition of radiolarian fauna. Radiolarian assemblages were collected on Mount Rettenstein (Northern Calcareous Alps) from a siliceous limestone and marl succession, deposited in a well-oxygenated basin a few hundred metres in depth on the continental shelf at the western edge of the Neotethys Ocean. Radiolarian research was complemented with elemental and isotope geochemistry on bulk carbonate samples. The siliceous microfaunas below and above the stage boundary consist of more than 80% sponge spicules and less than 20% radiolarians, with a strong predominance of the Order Spumellaria. The Nassellaria to Spumellaria abundance ratio ranges from 1:5 to 1:3. At the Sinemurian–Pliensbachian transition, a significant drop in diversity occurred, accompanied by a substantial change in relative abundances of radiolarian taxa. The most severely affected groups were surface-dwelling radiolarians (Angulobrachiidae, Hagiastridae, Pantanelliidae; mostly *Gorgansium*, Poulpidae and Ultranaporidae), which almost or completely disappeared. In contrast, *Archaeocenosphaera*, *Praeconocaryomma*, *Zhamoidellum* and *Lantus* became abundant and were apparently the most resistant to environmental stress. The changes in radiolarian assemblages were local and probably induced by the end-Sinemurian sealevel drop that transformed the area into a semi-enclosed basin with restricted ocean circulation. The exchange of water masses and thus radiolarian faunas with the open sea was reduced and their productivity may have been lowered by the lower inflow of fertile waters from the ocean.

Key words: Radiolaria, palaeoecology, Early Jurassic, Western Tethys, taxonomic composition, environmental crisis.

THE late Sinemurian to early Pliensbachian time interval was a period of climate, environmental and oceanographic changes. These changes are associated with carbon isotope excursions (CIE): a positive CIE in the *raricostatum* Ammonite Zone (e.g. Jenkyns & Weedon 2013), a positive CIE in the *ibex* Ammonite Zone (e.g. Mercuzot *et al.* 2020) and, between these two positive excursions, the most prominent negative CIE, named the Sinemurian–Pliensbachian Boundary Event (S-PBE; Korte & Hesselbo 2011), which has been documented at several locations in the Tethyan Realm (e.g. Hesselbo *et al.* 2000; Rosales *et al.* 2001, 2004; Jenkyns *et al.* 2002; van de Schootbrugge *et al.* 2005; Oliveira *et al.* 2006; Jenkyns & Weedon 2013; Franceschi *et al.* 2014, 2019; Gómez *et al.* 2016; Price *et al.* 2016; Ruhl *et al.* 2016; Peti *et al.* 2017; Danisch *et al.* 2019; Mercuzot *et al.* 2020; Schöllhorn *et al.* 2020a, 2020b; Cifer

et al. 2022). Although the trigger for the S-PBE is still largely unknown, it is postulated to be related to the ongoing break-up of Pangea and the opening of the Hispanic Corridor and the Viking Strait, or late phases of the Central Atlantic Magmatic Province (CAMP) volcanism (e.g. Korte & Hesselbo 2011; Price *et al.* 2016; Danisch *et al.* 2019; Franceschi *et al.* 2019; Schöllhorn *et al.* 2020a, 2020b; Storm *et al.* 2020).

This paper examines the impact of these environmental changes on radiolarian faunas living on the western edge of the Early Jurassic Neotethys Ocean. Studies on the distribution of recent radiolarians (e.g. Casey 1977; Boltovskoy *et al.* 2010; Boltovskoy 2017; Boltovskoy & Correa 2017) indicate that various radiolarian taxa (with different morphologies) characterize different water masses and that their distribution depends on physical and chemical factors

such as temperature, salinity, nutrient supply and water depth. Recent assemblages vary by the occurrence of species and by their relative abundances. Palaeoecological studies using a quantitative approach have been conducted on Triassic, Jurassic and Cretaceous radiolarians (Empson-Morin 1984; Pessagno & Blome 1986; Blome 1987; Baumgartner 1993; Hori 1993; Hull 1995; Kiessling 1996, 1999; Bartolini et al. 1999; Mekik 2000; Goričan et al. 2003; Carter & Haggart 2006; Baumgartner et al. 2023) and interpreted in terms of palaeolatitude, oceanic circulation and surface-water productivity. Detailed palaeoecological studies on radiolarian assemblages are still rare because estimates of diversity and relative abundances are meaningful only if the studies are based on very well-preserved material. Moreover, a series of successive good samples is needed to detect time-related variations. In contrast, general information indices (nassellarian/spumellarian abundance ratio and the proportion of sponge spicules) as reliable indicators of depositional depth and distance from the shelf (e.g. Kiessling 1996) are applicable to a wide range of preservation and thus are used more often.

Here we present fresh insights into radiolarian palaeoecology at the Sinemurian–Pliensbachian transition in the Western Tethyan Realm based on radiolarian assemblages paired with geochemical and sedimentological data from a limestone–marl sequence in the Northern Calcareous Alps. The studied assemblages contain almost 200 species belonging to 70 genera (Cifer & Goričan 2023a, 2023b) and are assigned to the upper Sinemurian *Canutus rockfishensis* – *Wrangellium thurstonense* and *Jacus? sandspitensis* radiolarian zones and to the lower Pliensbachian *Canutus tipperi* – *Katroma clara* Radiolarian Zone (Cifer et al. 2022). The aim of this study is to evaluate changes in the diversity and relative abundances of radiolarian taxa and to determine which were the main environmental factors controlling the composition of radiolarian assemblages.

GEOLOGICAL SETTING

The study was conducted using slightly siliceous limestone samples, collected on Mount Rettenstein in the central part of the Northern Calcareous Alps (Fig. 1A). The study area belongs to the Upper Tirolic mega-unit (Frisch & Gawlick 2003) and comprises three superposed tectonic units. From bottom to top, these units are: (1) the
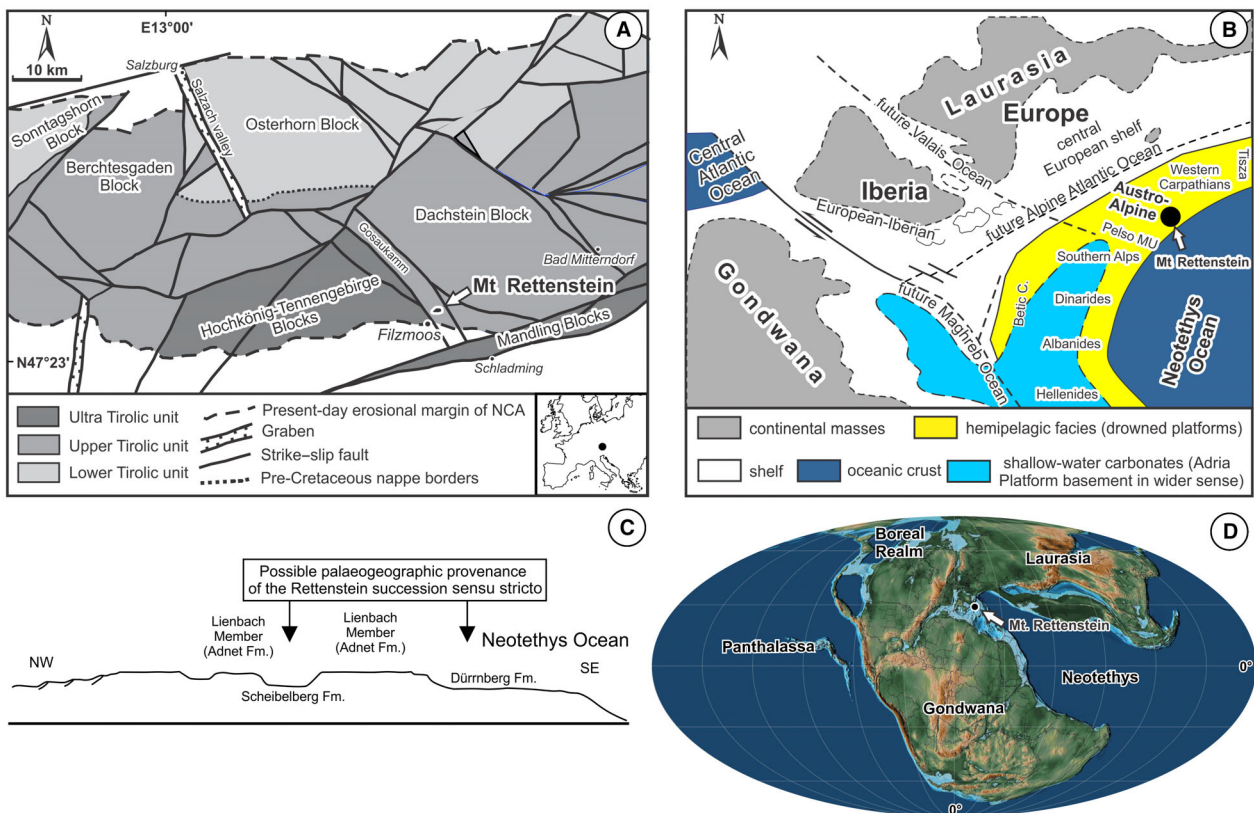

FIG. 1. Location of Mount Rettenstein. A, geological map of the central Northern Calcareous Alps (modified after Frisch & Gawlick 2003). B, plate reconstruction (modified after Gawlick & Missoni 2019). C, the palaeotopography of the Austroalpine domain in the late Hettangian to early Pliensbachian (after Gawlick et al. 2009). D, global palaeogeographical map during the Sinemurian–Pliensbachian (after Scotese 2002).

Werfen Imbricated Zone; (2) the Hallstat Mélange; and (3) the Rettenstein succession *s.s.* (Auer *et al.* 2009). The Rettenstein succession begins with a *c.* 100-m-thick succession of Lower Jurassic radiolarian-bearing siliceous limestone and marl. The overlying lithostratigraphic units are Pliensbachian–Toarcian Adnet-like red condensed marly siliceous limestone (Meister & Böhm 1993), Middle Jurassic red marly limestone of the Klaus Formation, the Middle–Upper Jurassic Rettenstein Debris Flow and upper Oxfordian radiolarite of the Ruhpolding Radiolarite Group. The entire top of the mountain is made up of several tens of metres of Upper Jurassic (Kimmeridgian–Tithonian) reef-slope limestones of the Plassen Formation (for a synthetic log of the Rettenstein succession *s.s.*, see Cifer *et al.* 2020, fig. 4). The topic of this study is the Lower Jurassic siliceous limestone and marl succession deposited in the westernmost parts of the Neotethys Ocean (Fig. 1B, D). A more exact tectonic affiliation and palaeogeographic provenance of the Rettenstein succession *s.s.* (Auer *et al.* 2009) remains unclear. It cannot be determined from structural and facies analyses alone whether the succession belongs to the intra-platform or the ocean-ward setting (Cifer *et al.* 2020; Fig. 1C).

MATERIAL & METHOD

The sampled Weitenhausgraben section (47°27′09.21″N, 13°32′56.10″E) is located on the southern flank of Mount Rettenstein. The section consists of siliceous limestone and marly limestone layers. The sampling was focused on radiolarians, thus only harder layers with higher carbonate and silica content were collected and used for analyses. Altogether 40 samples were collected (Fig. 2). Radiolarians were extracted with the standard method for carbonate rocks. The samples were crushed to walnut size and dissolved in acetic acid (8%) for 24 h. Then the residues were sieved through a 63 µm mesh. After drying, the sieved residues were split into four homogenous aliquots. One was kept for counting, whereas the other three aliquots were placed in 3% hydrofluoric acid for 10 min to free the radiolarians from clay minerals sticking to the skeletons. The radiolarians were examined under an Olympus SZ61 stereomicroscope with ×50 magnification. A detailed observation of radiolarian specimens was performed with a JEOL JSM-T330A scanning electron microscope.

Six samples yielded well-preserved radiolarian assemblages: four (Rö437, Rö438, Rö439, Rö440) belong to the
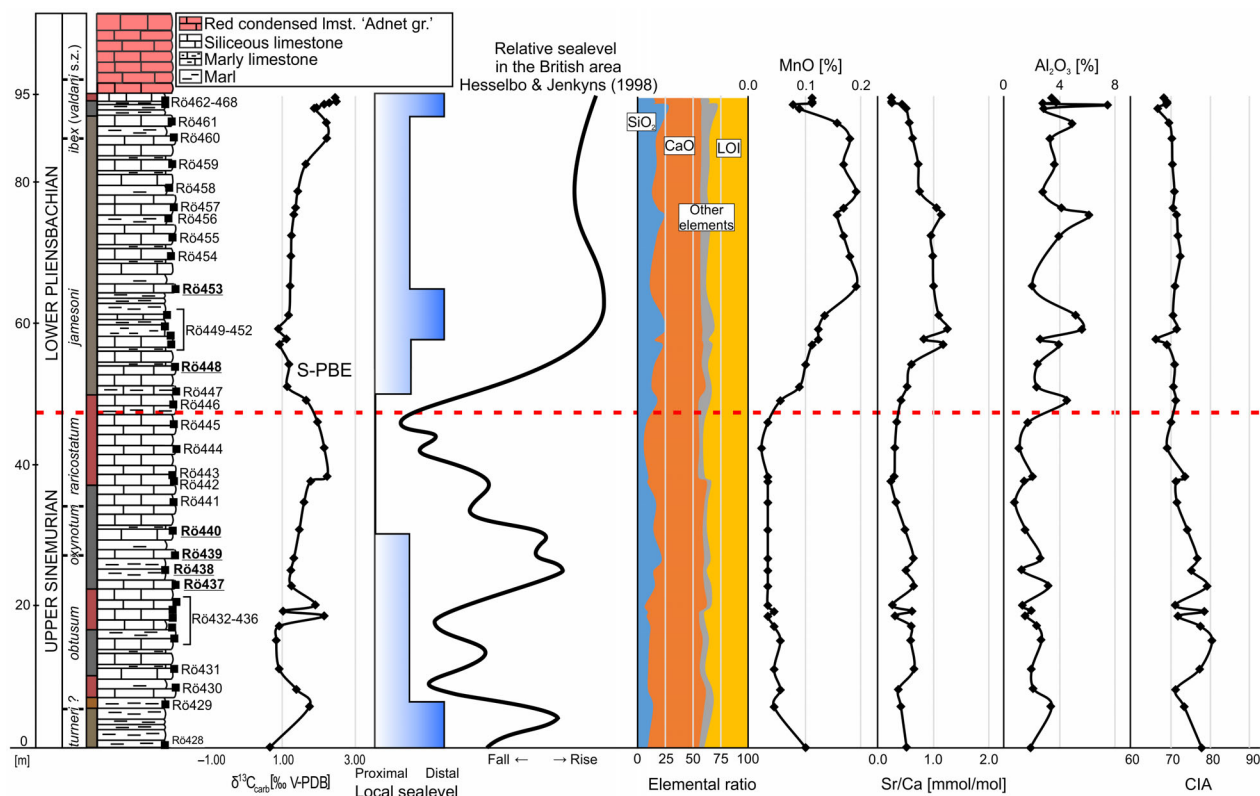

FIG. 2. Stratigraphic chart with stable carbon isotopes, local relative sealevel, relative sealevel of the British area (Hesselbo & Jenkyns 1998), proportions of SiO₂, CaO, other elements and LOI, MnO, Sr/Ca, Al₂O₃ and chemical index of alteration (CIA) curves. *Abbreviations*: LOI, loss on ignition; S-PBE, Sinemurian–Pliensbachian Boundary Event; V-PDB, Vienna Pee Dee Belemnite.

upper Sinemurian *Canutus rockfishensis* – *Wrangellium thurstonense* and *Jacus*? *sandspitensis* radiolarian zones and two samples (Rö448 and Rö453) to the lower Pliensbachian *Canutus tipperi* – *Katroma clara* Radiolarian Zone (Cifer *et al.* 2022). The diversity was determined on the basis of a recently published thorough taxonomic study (Cifer & Goričan 2023a, 2023b).

Taxon quantitative analysis was conducted using the stereomicroscope. In the first step, sponge spicules and radiolarians were counted together, until 500 specimens had been counted. The percentage of spicules was then calculated based on that number. In the second step, only radiolarians were continued to be counted until the number of 500 specimens had been reached. Only genera and higher taxonomic categories were considered because most radiolarians cannot be accurately identified with a stereomicroscope at the species level.

Stable carbon and oxygen isotope analyses of bulk carbonate samples were conducted at the Institute for Geological and Geochemical Research, Research Centre for Astronomy and Earth Sciences, Budapest. The carbon and oxygen isotope compositions of the carbonate samples were determined using an automated carbonate preparation device (GASBENCH II) and a Thermo Finnigan delta plus XP continuous-flow mass spectrometer. Three laboratory standards, calibrated using the NBS-18, NBS-19 and LSVEC reference materials (provided by the International Atomic Energy Agency) were used for sample standardization. The carbon and oxygen isotope compositions are expressed as $\delta^{13}C$ and $\delta^{18}O$ in ‰, relative to the Vienna Pee Dee Belemnite (V-PDB) scale. As a test of external precision, the Harding Iceland Spar (Landis 1983) sample was measured as unknown and yielded $\delta^{13}C$ and $\delta^{18}O$ values of -4.80 ± 0.05‰ and -18.55 ± 0.06‰ (n = 20 in five measurement series), respectively. These values are close to the published values of -4.80‰ and -18.56‰, respectively (Landis 1983).

Samples for the chemical analysis for major (SiO_2, Al_2O_3, Fe_2O_3, MgO, CaO, Na_2O, K_2O, TiO_2, P_2O_5, MnO) and minor (Cr_2O_3, Ba, Ni, Sr, Zr, Y, Nb, Sc) elements of bulk carbonate samples were prepared with an agate mortar. The analyses were performed by Bureau Veritas, Vancouver, British Columbia, Canada using inductively coupled plasma atomic emission spectroscopy (ICP-AES). The dissolution of the whole rock samples was accomplished using lithium borate fusion. Six duplicates and seven standards were used for quality control. All samples except Rö463 were analysed for major and minor elements.

Rock samples and the illustrated material are deposited at the Ivan Rakovec Institute of Palaeontology Research Centre of the Slovenian Academy of Sciences and Arts in Ljubljana, Slovenia.

RESULTS

Lithostratigraphy & microfacies

The section consists of alternating layers of marl, marly limestone and siliceous limestone containing more than 10% of dispersed silica. The limestone is mostly well bedded, with a bed thickness of up to 25 cm (exceptionally more) and an average thickness of 10 cm. The succession is 95.5 m thick and predominantly grey to brownish-grey marl, marly limestone and siliceous limestone, with three intervals consisting of red limestone (Fig. 2). Two thinner reddish intervals occur at the base of the section. The third reddish interval is *c.* 20 m thick and corresponds to the top of the Sinemurian and the lowermost beds of the Pliensbachian. The overlying lithology is again predominantly grey marl with grey limestone beds. However, the colour is lighter, more beige grey than the underlying grey layers. Only the uppermost beds, just below the red condensed limestone of the Adnet-like formation, are again red. At 60 m, an 80-cm-thick limestone layer occurs, which is very prominent in this section. Thin sections of the upper and lower parts of this bed show no laminations and no changes in grain size; the microfacies in both is a structureless wackestone, similar to other sampled beds. The studied section ends at the beginning of the red condensed Adnet-like limestone with ammonites (Meister & Böhm 1993).

Radiolarian and sponge spicule-bearing mudstones to wackestones are the dominant microfacies (Fig. 3) throughout the entire section. In the lower part of the section, the microfacies type is more finely grained, whereas it is coarser grained in the upper part of the section (for additional photographs of the microfacies see Cifer *et al.* (2020, fig. 5) and Cifer *et al.* (2022, fig. 4)). The micritic matrix has some clay admixture and is bioturbated. The grains are microfossils and undeterminable carbonate grains. The most common microfossils are radiolarians and sponge spicules (Fig. 3). Still, they are not abundant in every sample. Some samples also contain thin-shelled bivalves, foraminifers or echinoderms. Stylolites and reddish colouring are evident only in a few samples, chiefly in the wackestone microfacies. Mudstone does not show any evident recrystallization, although slight silicification can be recognized around radiolarians and sponge spicules in some samples. Wackestone, in comparison, shows some degree of microsparitization in a few samples in the shape of small sparitic grains spread throughout the micritic matrix. However, the recrystallization process is very weak and did not develop to a true microsparite.

The investigated Sinemurian–Pliensbachian succession belongs to either the Scheibelberg Formation or the
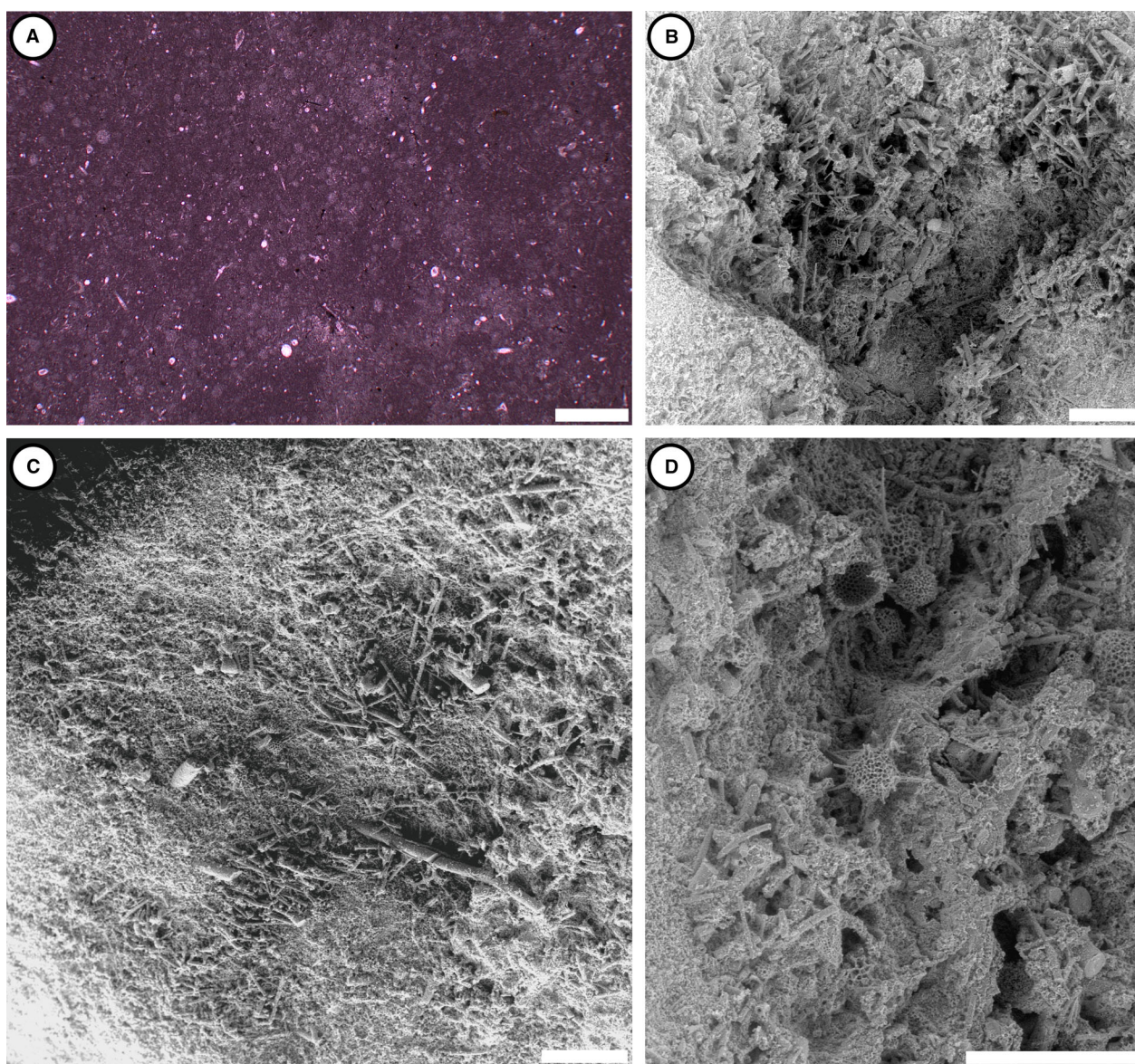
FIG. 3. A, wackestone microfacies of sample Rö438 with areas of higher density of radiolarians and sponge spicules in the thin section. B–D, acetic-acid etched surface of sample Rö438 with well-preserved radiolarians and abundant sponge spicules. Scale bars represent: 1 mm (A); 500 μm (B–D).

Dürrnberg Formation (Fig. 1C). Gawlick *et al.* (2009) interpreted the Dürrnberg Formation as a pelagic basin facies in the Hallstatt Zone, representing a deeper shelf environment on a relatively distal continental margin. The Scheibelberg Formation is, in contrast, interpreted as a hemipelagic cherty limestone deposited more proximally, in a basin succeeding the Late Triassic Eiberg Basin, located behind a morphological high that separated the basin from the open ocean (Fig. 1C).

In the Early Jurassic Western Tethys, the contribution of calcareous plankton to the pelagic carbonates was low and limestone–marl alternations resulted primarily from the cyclical export of carbonate mud from shallow-water carbonate platforms (Mattioli & Pittet 2002). In the studied section, calcareous plankton were very rare to rare (Cifer *et al.* 2022). No large carbonate platforms or ramps have been recognized in the Northern Calcareous Alps for that time interval. Only morphological highs existed where carbonate was produced. Hence, the carbonate in the section under study must have originated from these highs and accumulated as periplatform ooze in the basin. A suitable candidate for providing carbonate to the basin is the crinoid- and echinoderm-rich Lienbach Member of the Adnet Limestone (Fig. 1C) that, during the

Sinemurian and earliest Pliensbachian, was deposited on top of the drowned Rhaetian reefs (Böhm 2003; Gawlick *et al.* 2009 and the references therein). The thin sections of the studied samples also yielded rare echinoderms, which further support the topographic-high origin of the carbonate (Fig. 1C).

Elemental & stable isotope geochemistry

The results of stable isotope and geochemical analyses performed on bulk carbonate samples are given in Table S1 and Figure 2. All samples were analysed for the content of some major (SiO_2, Al_2O_3, Fe_2O_3, MgO, CaO, Na_2O, K_2O, TiO_2, P_2O_5, MnO) and minor elements (Cr_2O_3, Ba, Ni, Sr, Zr, Y, Nb, Sc). The majority of analysed elements show significant differences in the amount of the respective elements between the upper Sinemurian and lower Pliensbachian parts of the section. All analysed elements, except CaO and MgO, have higher values in the lower Pliensbachian, indicating a lower carbonate production or higher terrigenous input.

The SiO_2 content ranges from 5.36% in sample Rö444 (referred to the upper Sinemurian, *raricostatum* Ammonite Zone) to 27.41% in sample Rö464 (referred to the lower Pliensbachian, *ibex* Ammonite Zone), although most samples have an SiO_2 content of between 10% and 20% (Fig. 2). Only in sample Rö462 is the SiO_2 content higher, at 44.86% (Table S1), which is considerably more than in other samples, and a consequence of diagenetic alteration. Generally, although the average SiO_2 is higher in the lower Pliensbachian, there are also segments with lower contents of SiO_2 in the lower Pliensbachian and segments with higher values in the upper Sinemurian (Fig. 2). The SiO_2 to Al_2O_3 chart (Table S6; after Barbera *et al.* 2006) indicates that the majority of the silica has a biogenic origin. Aluminium, titanium and potassium generally originate from the aluminosilicate detritic phase and are therefore a good indicator of terrigenous input. Al_2O_3 ranges from 0.88% to 6.88%. The amount of Al_2O_3 is generally higher towards the top of the studied section, with only a few samples not following the trend. A similar trend is observed for TiO_2 and K_2O, with values usually also increasing towards the top. The TiO_2 content ranges from 0.05% to 0.34%, while the K_2O content ranges from 0.22% to 2.48%. The common terrigenous origin of these elements is further supported by the high mutual correlation coefficient (r) for Fe_2O_3 (r = 0.95 for Al_2O_3, r = 0.95 for TiO_2 and r = 0.94 for K_2O; Table S2). The correlation coefficient for Na_2O is also relatively high and indicates a common origin of Al_2O_3, TiO_2, K_2O, and Fe_2O_3. The Na_2O content ranges from 0.03% to 0.23%. According to the Fe_2O_3/TiO_2 versus $Al_2O_3/(Al_2O_3 + Fe_2O_3)$ diagram proposed by Girty *et al.* (1996), the non-biogenic, non-carbonate component of the samples was plotted in the area of the 'continental margin' and the shared area between 'continental margin' and 'pelagic' (Table S7). A terrigenous origin is also indicated by the Fe_2O_3/TiO_2 versus $Al_2O_3/(Al_2O_3 + Fe_2O_3 + MnO)$ diagram of Boström (1973) in which the siliciclastic component is plotted on the 'terrigenous' line (Table S8). The content of manganese (MnO) in the analysed samples ranges from 0.03% to 0.18% and, similar to other elements, is higher towards the top (Fig. 2). This is not the case, however, for phosphorus (P_2O_5), which has low correlation coefficients (Table S2) for 'terrigenous' elements. Phosphorus in the sediment could be related to increased biogenic activity in the basin or to increased volcanic activity (Halamić *et al.* 2005). Barium is also an element that can reflect productivity. We calculated excess barium (Ba_{xs}) after Casacci *et al.* (2016) as a palaeoproductivity proxy. The values exceeded 40 p.p.m. only in two samples and no sample exceeded 100 p.p.m., which is not sufficient to interpret any productivity variations.

The contents of the measured minor elements are low throughout the section. Cr, Sc and Zr have high mutual correlation coefficients as well as high correlation coefficients for the terrigenous components. They are usually transported into the basin in the form of detritus bound to clay minerals. Yttrium, in contrast, has no significant mutual correlation with any other element. Strontium has the highest correlation coefficient with manganese (r = 0.58) and phosphorus (r = 0.50). Both manganese and strontium have a low negative correlation with CaO and are therefore not entirely dependent on the carbonate phase. They also have a moderate correlation with the terrigenous components, and could thus also be partly derived from this origin. Manganese and strontium also have elevated values in the upper part of the succession that decrease again in the uppermost samples.

The chemical index of alteration (CIA) was calculated to estimate the degree of chemical weathering and precipitation rates on the adjacent land. A higher CIA indicates higher precipitation rates. The index is usually calculated with the formula $Al_2O_3 \times 100/(Al_2O_3 + CaO + Na_2O + K_2O)$ in molar proportion. Schöllhorn *et al.* (2020b) proposed replacing the CaO values with Na_2O in order to ignore the environmental and diagenetic influence on carbonate (limestone), which is the main component of the sediments in this study. The updated formula is then $Al_2O_3 \times 100/(Al_2O_3 + 2 \times Na_2O + K_2O)$. The CIA is higher at the base of the section, where some major shifts occur. The general trend shows a decrease towards the top, with a relatively stable upper part of the section, meaning that in the early Pliensbachian the intensity of chemical weathering in the source area was lower than in the late Sinemurian (Fig. 2; Table S4).

Bulk $\delta^{13}C$ values range from 0.64‰ to 2.22‰ (Fig. 2; Table S5). A distinct negative excursion was detected in the middle to upper part of the studied section where the values fall from 2.00‰ to 1.05‰. The shift to lower

values starts at *c.* 40 m and reaches its minimum at *c.* 50–60 m. After the drop, the values gradually increase and reach 2.22‰ in the uppermost parts of the section. Another part with evidently lower values is located at the base of the section where the values go as low as 0.64‰ and then gradually rise towards the high at 40 m. The curve changes gradually, only some fluctuations in the magnitude of 1‰ appear in the lower part of the section, at *c.* 2 m. The values are gradually increasing in the upper part of the section. We correlated the negative CIE in the middle part of the section with the supra-regional Sinemurian–Pliensbachian boundary event of Korte & Hesselbo (2011) and used it as a stratigraphic marker to establish the Sinemurian–Pliensbachian boundary in the studied section (Cifer *et al.* 2022). In contrast, $\delta^{18}O$ values show no clear trend ascribable to changes in temperature. In addition, a strong negative correlation with detrital elements is evident for the $\delta^{18}O$ values. Detrital-rich layers are more susceptible to diagenetic alteration, which indicates that the $\delta^{18}O$ signal is diagenetically altered and will thus not be used for further interpretations concerning palaeotemperature and palaeoecology.

Taxonomic composition of siliceous assemblages

Preservation & diversity. The abundance of siliceous microfossils in the studied thin sections varies from absent to more than 10% of the rock. All samples were processed to extract siliceous microfossils. For further studies, we selected only six samples (the underlined samples in Fig. 2) in which the preservation and abundance of isolated radiolarian specimens were suitable for stratigraphic and palaeoecological analyses. The selected radiolarian assemblages are equally well preserved. The preservation index (PI) of the studied faunas is determined as very good (PI = 2 according to Kiessling 1996). More than 90% of all individuals could be identified using the scanning electron microscope. The numerical diversity of the assemblages is supposedly not affected and the quantitative analyses are meaningful. We note that all these radiolarian-rich samples were obtained from grey limestone beds and in intervals with higher SiO_2 content (Fig. 2) that may indicate periods of relatively high biological productivity.

We present the taxonomic richness as the total number of genera (Table 1) and species (data from Cifer & Goričan 2023a, 2023b) and also specify the number of genera and species of each order (Fig. 4). In the majority of samples, although not all (see sample Rö439 in Fig. 4), the number of nassellarian taxa exceeds that of spumellarians. If we include Entactinaria in Spumellaria, the nassellarian/spumellarian (N/S) diversity ratio is close to 1, as

is the case in most water depths except for the extremes (e.g. Empson-Morin 1984). Only in the upper two samples Rö448 and Rö453 is the N/S diversity ratio somewhat higher, although it remains below 1.5. We consider that these differences are too small to be statistically meaningful and thus exclude the variations in the N/S diversity ratio from further interpretation.

In the studied samples, a drop in diversity at the species and genus levels can be observed at the Sinemurian–Pliensbachian boundary. The lowest diversity occurs in sample Rö448, directly above the boundary, while an increase can be observed in sample Rö453. In general, Sinemurian samples (Rö437, Rö438, Rö439, Rö440) are more diverse and contain up to 90 species belonging to 46 genera (sample Rö438), whereas the Pliensbachian samples (Rö448 and Rö453) contain only 29 species belonging to 17 genera and 58 species belonging to 32 genera, respectively. The biggest drop in diversity across the boundary is observed in Spumellaria. Nassellaria and Entactinaria are less affected, but their diversity is reduced as well.

Relative abundance of sponge spicules & radiolarian orders. The proportion among larger groups is the first general information used in analyses of relative abundances. The siliceous microfauna of all six samples similarly consists of an extremely high percentage (83.8–95.2%) of sponge spicules (Fig. 5). More than 80% of sponge spicules belong to the group of monaxone microscleres. Other groups are megascleres, triaxon microscleres, tetraxon microscleres, rhaxes and desmas (Fig. 6). A relatively high abundance of sponge spicules indicates shallower and more proximal (shelf) conditions of sedimentation (Kiessling 1996). Proximal conditions are also indicated by the presence of tetraxon spicules and rhaxes that are typical of reef sponges (Demospongiae; Murchey 2004). The presence of large monaxon spicules is also indicative of shallower waters (Murchey 1990, 2004).

The abundance ratio between Nassellaria and Spumellaria is also a general index that can be obtained from faunas with all preservation levels. As in all previous studies on radiolarian palaeoecology, we interpret Spumellaria and Entactinaria as a single group. All radiolarian faunas under study are dominated by specimens of Spumellaria together with Entactinaria. Nassellaria represent only from 14.79% to 33% and their relative abundance rises slightly from the base towards the top of the section (Fig. 7). The upper Sinemurian samples yield an N/S abundance ratio from 1:3 to 1:4.5, whereas the lower Pliensbachian samples a ratio of *c.* 1:2. The N/S ratio is positively correlated with bathymetry or distance from the shelf (Kiessling 1996). The obtained values are thus in line with the relatively shallow pelagic environment

TABLE 1. Occurrence of radiolarian genera in the studied samples.

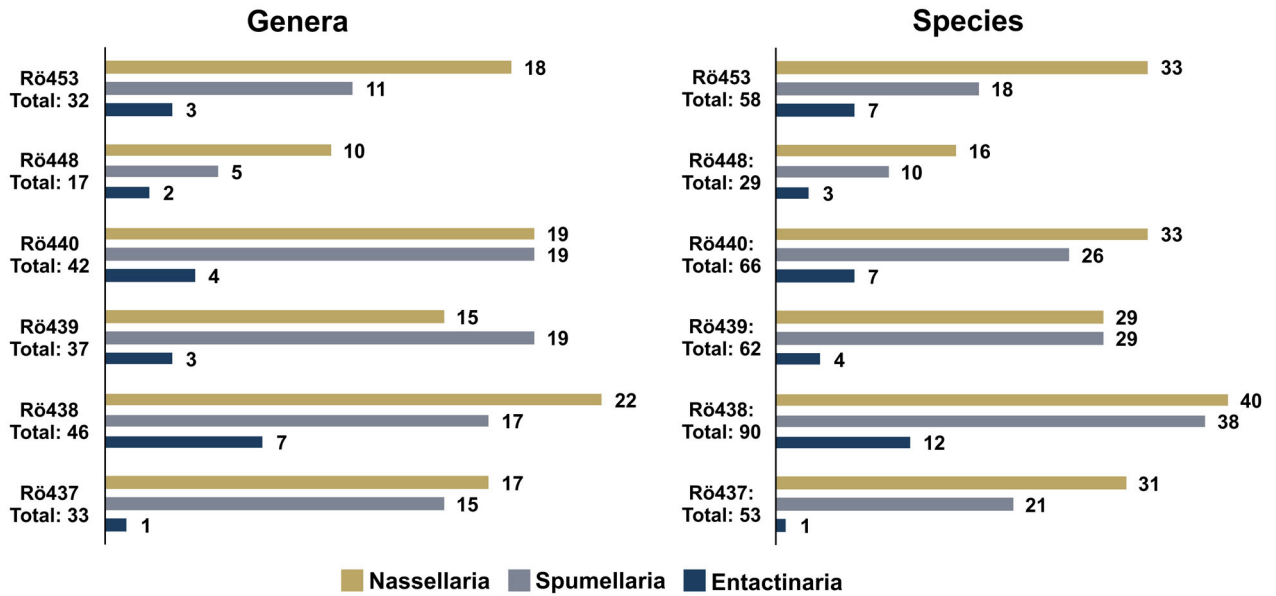| Order	Genus	Rö437	Rö438	Rö439	Rö440	Rö448	Rö453
Entactinaria	*Empirea*		•				
	Japonisaturnalis						•
	Palaeosaturnalis		•	•	•		
	Praehexasaturnalis		•	•	•		
	Pseudacanthocircus		•				
	Pseudoheliodiscus		•		•	•	•
	Stauracanthocircus		•				
	Stauramesosaturnalis					•	
Spumellaria	*Acaeniotylopsis?*	•	•	•			
	Archaeocenosphaera	•	•		•	•	•
	Beatricea?	•	•	•	•		
	Becus?		•	•	•		
	Charlottalum		•	•	•		
	Crucella	•	•	•	•		•
	Danubea	•	•	•	•	•	•
	Gorgansium	•	•	•	•		
	Hexapyramis?	•			•		
	Liassobetraccium		•	•	•		
	Loupanus	•	•	•	•		•
	Mendacastrum?	•	•	•	•	•	•
	Novamuria						•
	Orbiculiformella	•	•	•			
	Pantanellium		•	•	•	•	•
	Paronaella	•	•	•	•		
	Paurinella	•	•				
	Praeconocaryomma	•	•		•	•	•
	Tetractoma	•			•		
	Tetrapaurinella	•		•			
	Thurstonia?		•	•	•		•
	Tiperella?		•		•		
	Tozerium	•	•	•	•		•
	Udalia?	•	•	•	•		
Nassellaria	*Anaticapitula*	•	•	•	•	•	•
	Ares		•	•	•		•
	Atalantria	•	•		•		
	Bagotum	•				•	•
	Bipedis	•	•	•	•		
	Broctus	•	•	•	•		
	Canoptum	•	•				•
	Doliocapsa	•	•		•	•	•
	Droltus	•	•	•	•		•
	Dumitricaella?						•
	Ectonocorys?		•				
	Farcus	•	•	•	•		•
	Foremania	•	•	•		•	•
	Haeckelicyrtium		•				
	Helvetocapsa					•	
	Katroma	•	•	•	•		•
	Lantus					•	
	Napora	•	•	•	•		
	Naropa						•
	Parahsuum	•	•	•	•	•	•
	Pleesus				•		
	Podocapsa?						•
	Pseudoeucyrtis	•					
	Pseudoristola		•				
	Reticulotubulus?			•	•		
	Saitoum	•	•	•	•	•	•
	Squinabolia		•		•		
	Tipiforma	•	•	•	•		
	Trexus	•	•	•	•		•
	Turritus		•				
	Wrangellium	•		•	•		
	Zhamoidellum				•	•	•

FIG. 4. Radiolarian diversity through the section (for data on the occurrence of genera, see Table 1; species occurrence data are from Cifer & Goričan 2023a, 2023b).
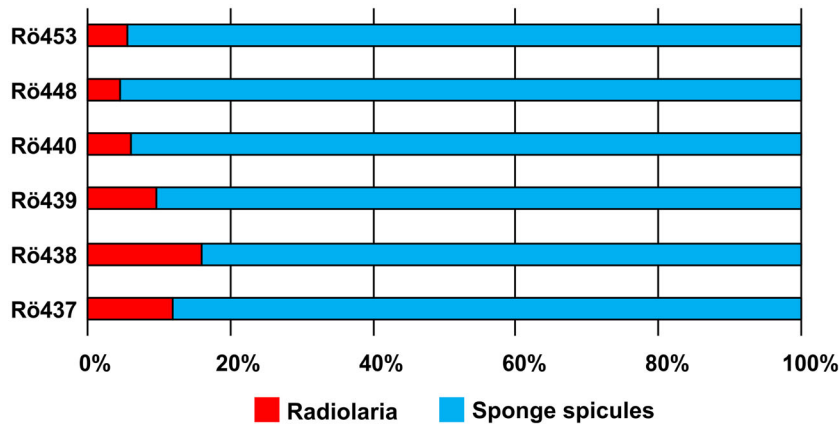

FIG. 5. Relative abundance of radiolarians and sponge spicules.

inferred from the high quantity of sponge spicules. The minor vertical fluctuations in the N/S ratio (Fig. 7) are not sufficient to be interpreted in terms of palaeodepth.

Relative abundance of radiolarian families & genera. For relative abundances, we used the radiolarian counting data in Table 2. Nassellaria were divided into 13 groups, of which each represents a family or a group of families or genera (Fig. 8). These groups are merged into larger groups based on the number of segments (Fig. 8). Nassellaria show a significant break in their relative abundance between the base and the top of the studied section. Upper Sinemurian assemblages have a similar composition and are characterized by monocyrtid and dicyrtid nassellarians, which together account for up to

45% of all Nassellaria. The most abundant mono- and dicyrtid nassellarians are Poulpidae (*Saitoum*) and Ultranaporidae (*Bipedis, Anaticapitula, Napora*). The remaining nassellarians in the upper Sinemurian assemblages are represented by multicyrtid Nassellaria, whereas tricyrtids (Williriedellidae) are almost absent (Fig. 8). A vast proportion of multicyrtids in the upper Sinemurian belong to Bagotidae and Hsuidae (*Bagotum, Droltus, Parahsuum*). In the lower Pliensbachian, monocyrtid and dicyrtid nassellarians almost disappear; they represent only up to 6% of all Nassellaria in these samples. In contrast, Williriedellidae (*Zhamoidellum*) are the most abundant group in the lower Pliensbachian, where they represent up to 65% of all Nassellaria. Some changes are observed within multicyrtid Nassellaria as well (Fig. 8). The abundance of
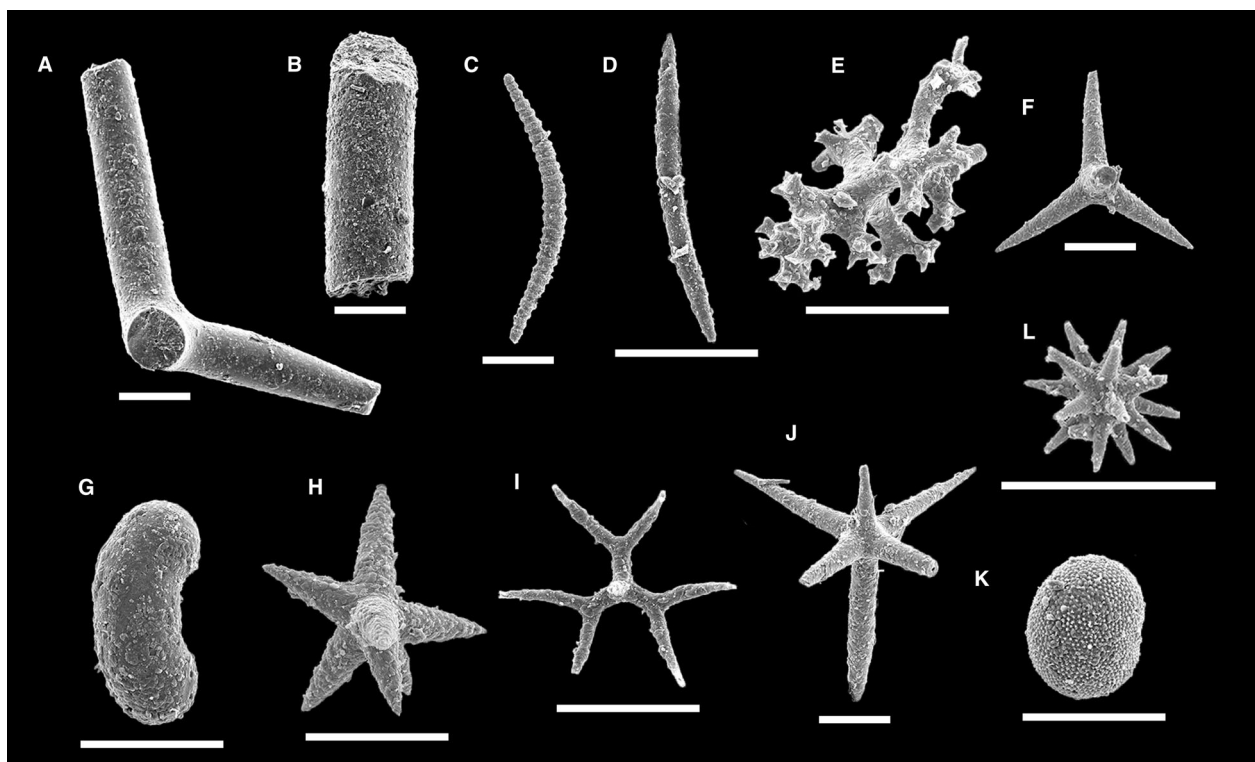
FIG. 6. Sponge spicules in the studied samples. A, triaxon megasclere, 2020_0003, sample Rö438. B, monaxon megasclere, 2020_0001, sample Rö438. C, monaxon microsclere, 2020_0019, sample Rö438. D, monaxon microsclere, 2020_0016, sample Rö438. E, desma, 2020_0024, sample Rö438. F, tetraxon, 2020_0029, sample Rö438. G, rhax, 2020_0034, sample Rö438. H, polyaxon, 2020_0040, sample Rö438. I, dichotriaene, 2020_0013, sample Rö438. J, triaxon, 2020_0031, sample Rö438. K, rhax, 2020_0033, sample Rö438. L, polyaxon, 2020_0039, sample Rö438. Scale bars represent 100 μm.
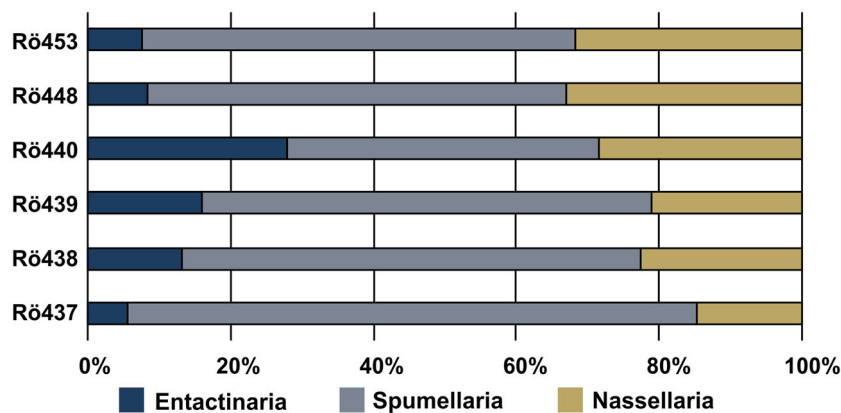

FIG. 7. Relative abundance of radiolarian orders.

Bagotidae and Hsuidae decreases in the Pliensbachian part of the section, whereas the number of representatives of the unnamed family pro-Eucyrtidiidae (predominantly *Lantus*) notably increases.

The counted Spumellaria and Entactinaria were divided into 10 groups representing a family or a group of families and genera (Fig. 9). Also in these groups, major changes in relative abundance are observed across the Sinemurian–Pliensbachian transition. A big drop in relative abundance from the Sinemurian to the Pliensbachian is observed for Eptingiidae (*Tozerium*), Pantanelliidae (predominantly *Gorgansium*), Angulobrachiidae (*Paronaella*, *Loupanus*), Emiluviidae (*Beatricea*, *Thurstonia*, *Udalia*), and for the group of Spumellaria and

TABLE 2. Number of specimens in the counted samples.

Order	Radiolarian group	Genus	Rö437	Rö438	Rö439	Rö440	Rö448	Rö453
Entactinaria	Eptingiidae	*Tozerium*	21	52	53	23	0	0
	Saturnalidae	*Palaeosaturnalis, Praehexasaturnalis* etc.	8	14	27	118	42	39
Spumellaria	Pantanelliidae	*Pantanellium*	0	17	4	0	29	16
		Gorgansium	235	96	143	92	0	0
	Xiphostylidae	*Archaeocenosphaera*	58	19	37	50	218	200
		Novamuria	22	9	5	2	9	9
	Conocaryommidae	*Praeconocaryomma*	22	3	12	7	22	66
	Veghicycliidae	*Orbiculiformella*	0	6	3	0	3	0
	Hagiastridae	*Crucella*	2	9	4	0	0	0
	Emiluviidae	*Beatricea*	2	1	1	1	0	0
		Thurstonia	3	15	8	7	0	0
		Udalia	5	33	13	3	2	2
	Angulobrachiidae	*Paronaella*	5	17	2	16	0	0
		Loupanus	8	46	40	5	0	0
Spumellaria & Entactinaria *incertae sedis*		*Mendacastrum* etc.	38	49	45	33	10	9
Nassellaria	Poulpidae	*Saitoum*	14	25	20	29	4	2
	Ultranaporidae	*Anaticapitula, Bipedis, Napora, Naropa* etc.	12	22	18	31	0	4
	Foremanellinidae	*Farcus*	3	4	1	6	2	1
	Deflandrecyrtiidae	*Haeckelicyrtium*	0	1	0	0	2	3
	Williriedellidae	*Zhamoidellum*	0	0	0	4	77	104
	Bagotidae?	*Trexus*	6	6	4	2	0	0
	Bagotidae & Hsuidae	*Parahsuum, Droltus, Bagotum*	30	39	48	49	42	22
	Canoptidae	*Canoptum*	0	3	0	0	0	0
	Parvicingulidae	*Atalantria*	0	1	0	6	0	0
	Eucyrtidiidae	*Katroma*	5	6	11	6	6	9
	Unnamed pro	*Lantus*	0	0	0	0	32	14
	Eucyrtidiidae	*Pseudoeucyrtis*	0	1	0	0	0	0
	Minocapsidae	*Doliocapsa*	1	0	1	2	0	0
	Nassellaria *incertae sedis*	*Ares, Turritus, Tipiforma, Reticulotubulus*	0	8	1	8	0	0
Total			500	500	500	500	500	500

Entactinaria *incertae sedis* (e.g. *Mendacastrum*). By far the biggest drop in relative abundance happens in the group of Pantanelliidae. They represent up to 54% of all Spumellaria and Entactinaria in the upper Sinemurian, but less than 9% in the lower Pliensbachian. Groups that show a major increase in relative abundance in the lower Pliensbachian are Xiphostylidae (predominantly *Archaeocenosphaera*) and Conocaryommidae (*Praeconocaryomma*). Xiphostylidae represent less than 20% in the upper Sinemurian, but up to 68% in the lower Pliensbachian. The relative abundance of Conocaryommidae increases from 5% in the upper Sinemurian to *c.* 20% in the lower Pliensbachian. Saturnalidae have a unique trend. They are rare in the three older Sinemurian samples Rö437–Rö439, representing only up to 7%, and become very numerous in the youngest Sinemurian sample Rö440 where they represent *c.* 32% of Spumellaria and Entactinaria. In the lower Pliensbachian, their abundance drops again to 12%.

DISCUSSION

Depositional environment

Mudstones to wackestones with radiolarians and sponge spicules are interpreted to indicate a deep shelf environment (Flügel 2004). The sedimentation of the studied succession may be interpreted as hemipelagic based on the micritic matrix mixed with terrigenous clay. The absence of current-related sedimentary structures indicates deposition in a low-energy environment, below the storm-wave base. In samples from which siliceous microfauna could be extracted, the proportions of radiolarians and sponge spicules were calculated. Sponge spicules are much more abundant than radiolarians and account for more than 80% of the total siliceous microfauna (Fig. 5). In radiolarian-bearing facies, such proportions indicate a relatively shallow environment, not exceeding a water depth of a few hundred metres (Kiessling 1996). Sponge
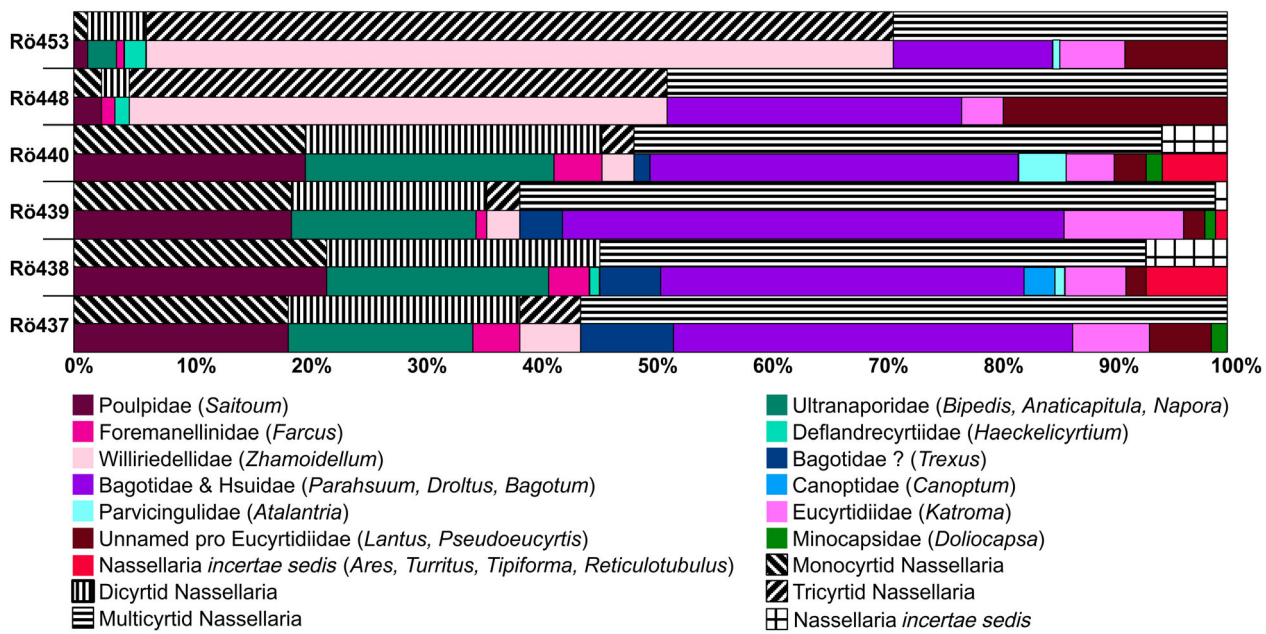
FIG. 8. Relative abundance of nassellarian groups. Each sample is represented by two rows. On the lower row, each colour represents a nassellarian family or a group of nassellarian families and genera. On the upper row, these groups are merged into larger groups based on the number of segments.
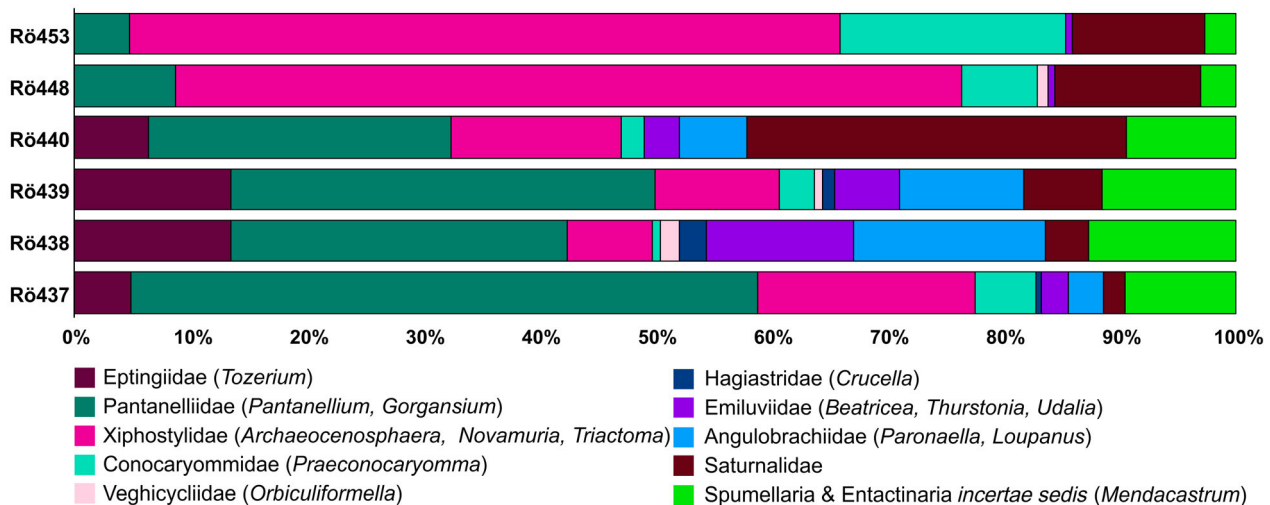

FIG. 9. Relative abundance of entactinarian and spumellarian groups.

spicules alone are also often used as indicators of palaeobathymetry because different groups of spicules prefer different depths. The predominance of small monaxones in the assemblages is consistent with a depth of a few hundred metres (Murchey 2004). In addition, sponge spicules and bioturbation indicate that the bottom waters were sufficiently oxygenated for benthos to thrive. A similar, relatively shallow water depth is also indicated by the predominance of Spumellaria over Nassellaria throughout the entire section (Fig. 7).

Sealevel changes

The investigated facies does not show any significant changes throughout the studied section, and the only parameter that could be used to interpret local sealevel changes is the limestone to marl ratio (Fig. 2). The amount of terrigenous elements (Al_2O_3, TiO_2, K_2O) correlates reasonably well with field estimations of the proportion of marl and may also reflect sealevel oscillations (Table S1). From the very low abundance of calcareous

plankton in this section (Cifer et al. 2022) we infer that carbonate mud is mostly derived from adjacent shallow-water areas. With a higher sealevel, the conditions become more distal with regard to the local carbonate source and the sedimentation consequently becomes marlier, while limestone layers are less frequent. When the sealevel drops, the position becomes more proximal, as reflected in a bigger proportion of limestone layers. Based on that, the local proximal–distal profile was constructed (Fig. 2), which shows a well-pronounced maximum proximality in the middle part of the section, below and just above the Sinemurian–Pliensbachian boundary.

The global sealevel during the Early Jurassic experienced several short-term fluctuations, although the general, long-term sealevel remained relatively constant until the early Toarcian; from the early Sinemurian towards the Pliensbachian a constant rise of the sealevel in the magnitude of tens of metres has been detected (Haq 2018). Several authors reported a significant short-term, end-Sinemurian, sealevel drop (Hallam 1988; Hesselbo & Jenkyns 1998; Haq 2018; Schöllhorn et al. 2020b), which caused the emergence of several carbonate platforms (Jenkyns 2020). This short-term drop was followed by a rise in the early Pliensbachian. The end-Sinemurian sealevel drop agrees well with our local sealevel reconstruction in the Northern Calcareous Alps (Fig. 2). In general, such a sealevel drop can be explained either by eustatic changes or a syn-sedimentary uplift. The fact that the onset of the intraoceanic thrusting in the Neotethys Ocean probably started around the Pliensbachian–Toarcian boundary (Karamata 2006) makes the eustatic sealevel drop more probable.

Productivity evaluation

In addition to temperature (latitude), nutrients and primary productivity are the most important factors defining the distribution pattern of modern polycystine radiolarians (Boltovskoy et al. 2017), and have also been proposed to explain the distribution of fossil taxa (e.g. Baumgartner 1987, 1993; Baumgartner et al. 2023). The investigated Sinemurian–Pliensbachian succession was deposited in low latitudes (Fig. 1B, D) and shows a relatively uniform hemipelagic facies, indicating water depths of a few hundred metres during the entire time interval studied.

The stratigraphic data in the upper part of the section enable us to determine the sedimentation rate with reasonable confidence. If we take the Sinemurian–Pliensbachian boundary at 50 m and the boundary between the *jamesoni* and *ibex* ammonite zones at 85 m of the section (Meister & Böhm 1993; Cifer et al. 2022; Fig. 2) and if we consider 2.4 Ma for the duration of the *jamesoni* Zone

(Storm et al. 2020), we calculate the sedimentation rate of lithified sediment at 14.6 m/Ma. For the lower 50 m of the section, age constraints are less precise. This interval probably encompasses the entire upper Sinemurian (*obtusum*, *oxynotum* and *raricostatum* zones) although the base of the section may reach the lower Sinemurian *turneri* Zone (Fig. 2). This means that the first 50 m correspond to a maximum duration of 3.7 Ma (according to Storm et al. 2020). The calculated average sedimentation rate of 13.5 m/Ma is comparable to the sedimentation rate in the upper part of the section. The actual sedimentation rate was probably lower than average in the reddish and higher in the grey facies (Fig. 2).

The proportion of silica in limestone beds is at most 25% (Fig. 2), which means that the accumulation rate of biogenic silica did not exceed 3.5 m/Ma. If, in addition, we subtract a minimum 85% of silica derived from siliceous sponges (Fig. 5) we obtain 0.5 m/Ma as the maximum accumulation rate of radiolarian skeletons. However, this figure is still too high because the 85% sponge spicules relate to the number of specimens, not to their weight percentage. The calculated value for radiolarians is thus considerably lower than in pure radiolarites. For example, sedimentation at a rate of 1 m/Ma was reported for Lower Jurassic radiolarian cherts in Japan (Hori et al. 1993).

The productivity varied through time as evidenced by variations in SiO_2 content and the better preservation of siliceous microfauna coincident with SiO_2 maxima (Fig. 2), but even in these maxima the radiolarian productivity was apparently lower than in coeval radiolarites deposited in high-fertility oceanic environments. One maximum appears in the upper Sinemurian and one in the lower Pliensbachian, both with a comparable proportion of silica. Facies characteristics and average sedimentation rates are relatively uniform throughout the section and hence show no major difference in the depositional environment between the upper Sinemurian and lower Pliensbachian parts of the section. The studied section formed part of a western embayment of the Neotethys (Fig. 1D). This palaeogeographic situation is similar to the present-day Gulf of Mexico and the Caribbean Sea that are also low-productivity regions (McMillen & Casey 1978).

The usual geochemical proxies for palaeoproductivity (such as Ba, P and MnO) do not show sufficiently significant shifts that can be used to interpret the production unambiguously. MnO values increase in the lower Pliensbachian (Fig. 2), but cannot be exclusively linked to changes in productivity because Mn can reside in or on clay minerals (Jenkyns et al. 2002), it can be a late diagenetic input, and is also sensitive to changes in redox conditions. Ba_{xs} in the studied section has a trend similar to MnO, with high values in the lower Pliensbachian

(Table S3). Barium, like manganese, is influenced by several factors and is not applicable in all ocean settings (Schoepfer *et al.* 2015). A possible explanation for these MnO and Ba fluctuations in terms of palaeoproductivity and the absence of correlation with positive radiolarian samples could be that the trend reflects an increase in phytoplankton production that potentially pre-dates the radiolarian recovery.

Unlike Ba and MnO, phosphorus behaves similarly to silica and thus potentially reflects the productivity of the siliceous microfauna. The lowest values are around the Sinemurian–Pliensbachian boundary and higher values appear below and above. The peak in the lower Pliensbachian is synchronous with the silica maximum, whereas the phosphorus maximum in the upper Sinemurian somewhat pre-dates the peak in silica content. However, the general trend agrees with the productivity evaluations.

Variations in taxonomic structure

The upper Sinemurian to lower Pliensbachian transition is marked by a significant drop in diversity. The number of species and genera decreases by more than 50% from the upper Sinemurian samples (Rö437, Rö438, Rö439, Rö440) to the oldest Pliensbachian sample Rö448 (Fig. 10). In sample Rö453, the diversity again increases and the number of identified species and genera returns

to similar numbers as in the upper Sinemurian assemblages. The drop in diversity across the stage boundary must have been related to an environmental stress that caused an extinction event and was then followed by a recovery. Many genera with a worldwide distribution and long stratigraphic range nearly or completely disappeared, including *Napora*, *Gorgansium*, *Orbiculiformella* and *Paronaella* (Table 1) that are dissolution resistant and which have a well-known range up to the Cretaceous (O'Dogherty *et al.* 2009). Moreover, we note that other well-preserved earliest Pliensbachian faunas (e.g. those from Haida Gwaii, British Columbia) are just as diverse as their Sinemurian counterparts (Carter *et al.* 2010). Hence, the inferred environmental stress was no doubt not a global phenomenon but must have affected only a limited geographical area.

Changes in relative abundances also indicate significant shifts through the Sinemurian–Pliensbachian transition (Fig. 10). The first event is an exceptionally high amount of Saturnalidae in the uppermost Sinemurian (sample Rö440). Musavu-Moussavou *et al.* (2007) argued that saturnalids prefer oligotrophic environments. However, the high abundance of Saturnalidae in sample Rö440 cannot be associated with certainty to nutrient-deprived waters because for the late Sinemurian a higher weathering intensity and thus continental runoff is interpreted based on the local CIA (Fig. 2). Supra-regional climate reconstructions also suggest higher temperatures and
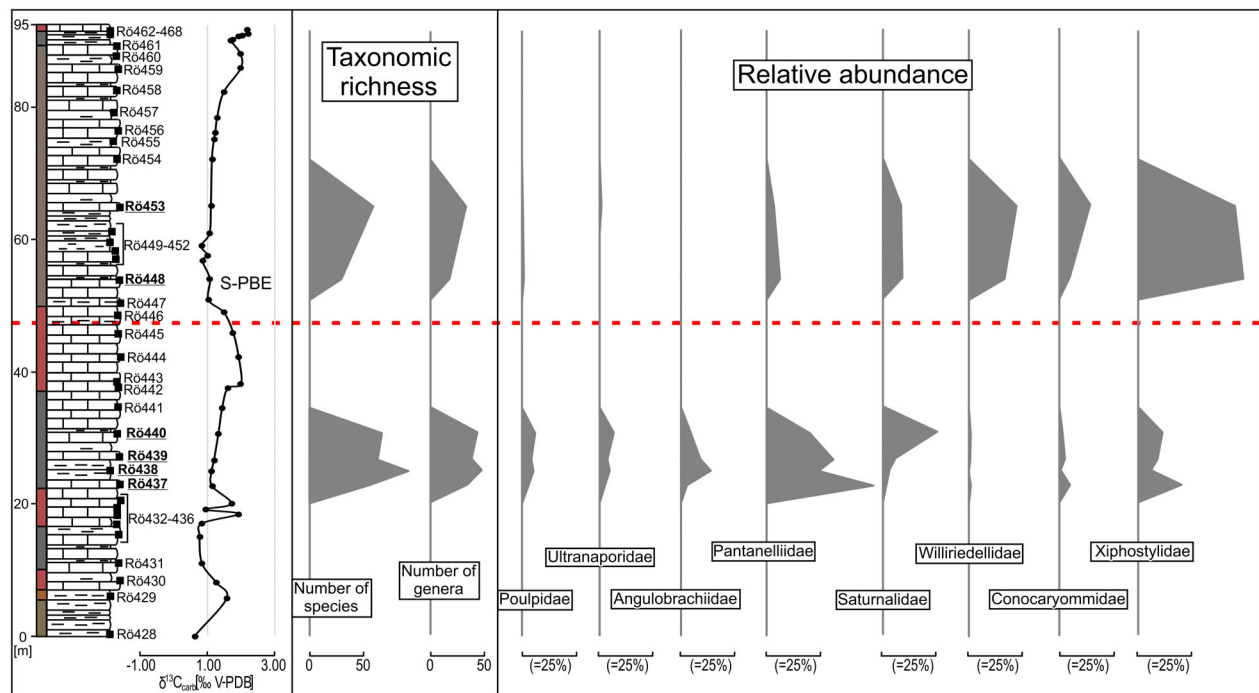

FIG. 10. Variation in taxonomic richness and relative abundance of characteristic radiolarian families. *Abbreviations*: S-PBE, Sinemurian–Pliensbachian Boundary Event; V-PDB, Vienna Pee Dee Belemnite.

precipitation for that time period (e.g. Korte & Hesselbo 2011; Duarte *et al.* 2014; Gómez *et al.* 2016; Price *et al.* 2016; Schöllhorn *et al.* 2020a, 2020b). In addition, the high relative abundance of *Gorgansium* (Pantanelliidae) also contradicts the interpretation of nutrient-deprived waters because this group of radiolarians is interpreted to be abundant in nutrient-rich environments (Baumgartner 1987; Hori 1993). A possible cause for the high numbers of saturnalids could be increased salinity or deposition in a more enclosed depositional environment. Sample Rö440 was taken from that part of the section where the limestone to marl ratio is higher, thereby indicating more proximal conditions (Fig. 2). Furthermore, the uppermost Sinemurian is interpreted to sustain a sealevel drop (Hesselbo & Jenkyns 1998; Haq 2018), which is in agreement with the sealevel interpretation of the Mount Rettenstein section. The most proximal conditions are connected to the lowest sealevel, and therefore possibly the highest salinity caused by higher evaporation and a limited connection to the open sea. Empson-Morin (1984) also reported high Saturnalidae numbers in samples that originated from an enclosed area with restricted oceanic circulation.

The second event is a major shift in relative abundances across the Sinemurian–Pliensbachian boundary, coinciding with the severe decline in diversity indicating an environmental crisis (Fig. 10). The most sensitive radiolarians disappeared, whereas more tolerant radiolarians survived and prospered during the recovery (Fig. 11). For Nassellaria, the most drastic decline in abundance occurs in monocyrtids (*Saitoum*) and dicyrtids (Ultranaporidae). The relative abundance of multicyrtids also decreases, but the drop is not as significant. The decrease of relative abundance of multicyrtid Nassellaria can mostly be attributed to Bagotidae and Hsuidae (Fig. 8). Spumellaria (Fig. 9) sensitive to this environmental stress are Pantanelliidae, particularly the genus *Gorgansium*. A decrease in relative abundance is also observed in Emiluviidae (*Udalia* and *Thurstonia*) and Angulobracchiidae (*Paronaella* and *Loupanus*). After the crisis, the most successful Nassellaria are Williriedellidae (*Zhamoidellum*) and somewhat less conspicuously *Lantus*, while the most successful Spumellaria are Xiphostylidae (*Archaeocenosphaera*) and Conocaryommidae (*Praeconocaryomma*). It could be argued that such a faunal composition with prevailing spherical Nassellaria and Spumellaria is the result of hydraulic sorting. However, limestone samples from Mount Rettenstein show no evidence of bottom currents to support this explanation.

A comparison with the vertical distribution of morphologically similar modern radiolarians (Casey 1977, 1979; Boltovskoy 2017) suggests that radiolarian taxa living in the upper part of the water column were most affected by the environmental crisis. For example, spumellarian genera *Crucella*, *Paronaella* and *Orbiculiformella*, the numbers of which shrink drastically in the Pliensbachian, are morphologically very similar to *Spongaster*, *Dictyocoryne*, *Heliodiscus* and *Spongotrochus* that are all common in shallow waters (Boltovskoy 2017). Among Nassellaria, *Anaticapitula*, *Bipedis*, *Farcus* and *Saitoum* have their numbers drastically decreased in the Pliensbachian. They are comparable to *Pterocanium*, *Pterocorys*, *Pterocyrtidium*, *Clathrocorys* and *Lipmanella* that are common in recent shallow waters (McMillen & Casey 1978; Boltovskoy 2017). The deep-dwelling (or, more probably eurybathic) radiolarians were apparently tolerant to the environmental stress and became relatively abundant when radiolarians living near the surface were eliminated. Casey (1977) postulated that the extinction of shallow-water radiolarians coincides with extinctions in phytoplankton groups, while deep-water forms fare better. During the S-PBE, Peti & Thibault (2022) observed in the Paris Basin a switch in dominance from shallow-water forms to deep-dwelling coccolith taxa, which is consistent with the changes observed in the radiolarian assemblages in our study.

In modern seas, high radiolarian diversity occurs in open-ocean environments, whereas near-shore areas are characterized by lower diversity and the predominance of very few species (e.g. Casey 1987; Boltovskoy *et al.* 2017). Such low-diversity neritic assemblages are also known from the fossil record, for example, from the Campanian of California, Texas and Romania (Empson-Morin 1984) and from the Upper Jurassic Lithographic Limestone (a typical epeiric-sea deposit) in southwest Germany (Zügel *et al.* 1998). As in the Pliensbachian samples from Mount Rettenstein, a notably high abundance of Williriedellidae was reported at these sites.

In previous studies on fossil radiolarians, Williriedellidae were considered ecologically tolerant and indicative of low-productivity areas (Baumgartner *et al.* 1992, 2023; Baumgartner 1993) as opposed to Pantanelliidae that indicate areas of high productivity (Baumgartner 1987, 1993; Hori 1993). We were unable to ascertain from the facies characteristics and estimates of the silica accumulation rate (see Productivity Evaluation, above) a considerable difference in productivity between the upper Sinemurian samples containing high proportions of Pantanelliidae and the lower Pliensbachian samples with high numbers of Williriedellidae. A decline in productivity across the stage boundary is, however, possible but needs to be related to other factors to explain the environmental deterioration and disappearance of many taxa.

We speculate that the critical kill mechanism was in fact most effectively operating during the times when the barren interval between samples Rö441 and Rö447 was deposited (Fig. 2). This assumption enables us to consider the sealevel drop as the main reason for environmental changes in the basin. The silica-poor interval of reddish
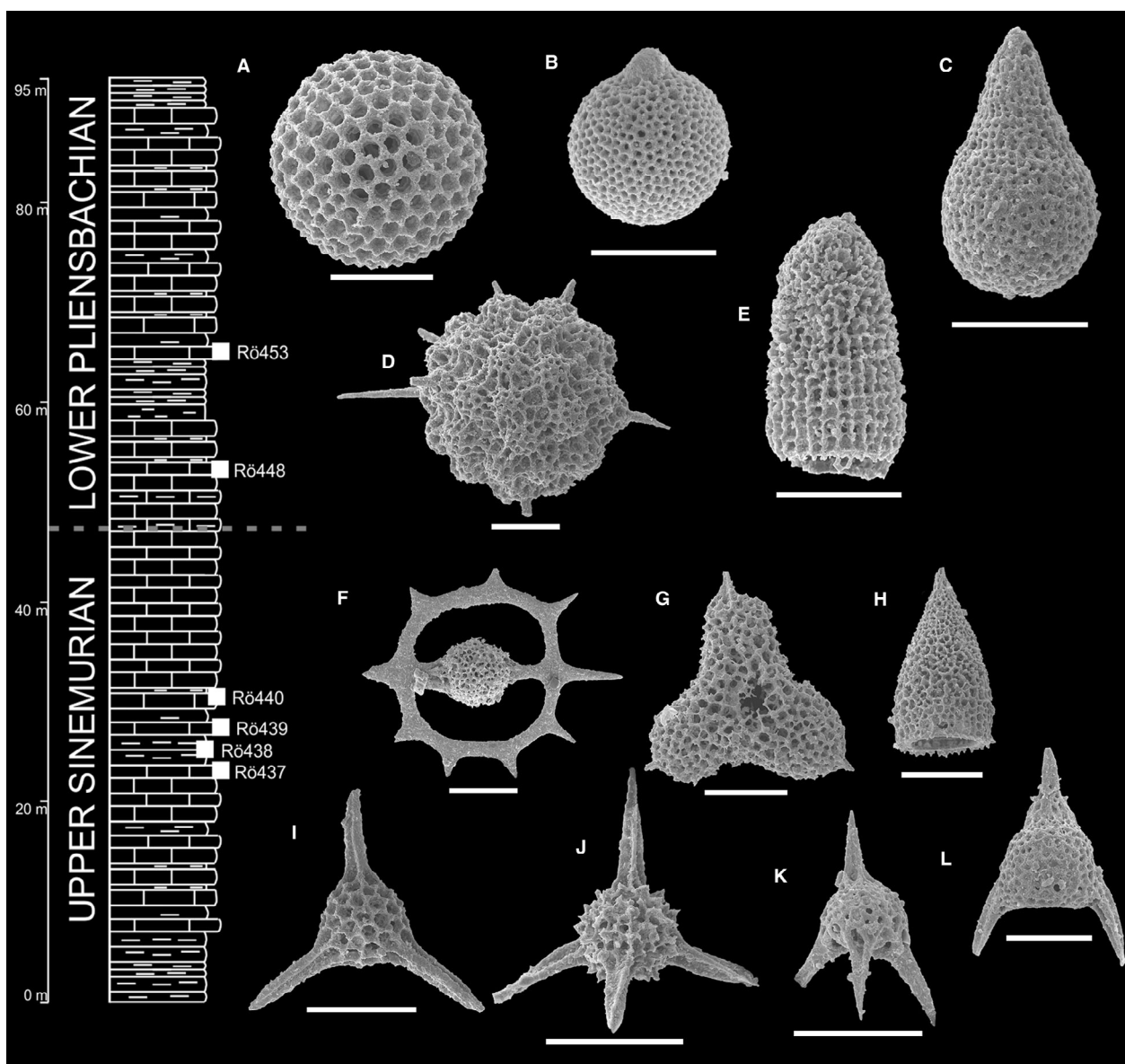
FIG. 11. Characteristic radiolarian genera that are abundant in the lower and upper part of the section, respectively. Specimen numbers and sample numbers are indicated. A, *Archaeocenosphaera ruesti* Pessagno & Yang; 193157, sample Rö438. B, *Zhamoidellum yehae* Dumitrica; 192697, sample Rö453. C, *Lantus praeobesus* Carter; 192406, sample Rö448. D, *Praeconocaryomma bajaensis* Whalen; 192508, sample Rö448. E, *Droltus sanignacioensis* Whalen & Carter; 193185, sample Rö453. F, *Palaeosaturnalis subovalis* Kozur & Mostler; 191006, sample Rö438. G, *Paronaella corpulenta* De Wever; 191013, sample Rö438. H, *Droltus laseekensis* Pessagno & Whalen; 191650, sample Rö439. I, *Gorgansium gongyloideum* Kishida & Hisada; 191422, sample Rö438. J, *Tozerium filzmoosense* Cifer; 192211, sample Rö440. K, *Saitoum* aff. *keki* De Wever; 191338, sample Rö438. L, *Bipedis horiae* Sugiyama; 192157, sample Rö440. Scale bars represent 100 μm.

limestone without marl interlayers indicates oligotrophic highly oxic conditions and is ascribed to the maximum proximality of the local depositional environment. This interval corresponds to the well-established regional sea-level low-stand in the *raricostatum* Zone (Hesselbo & Jenkyns 1998). Due to the drop in sealevel, the topographic highs could have acted as a barrier that diverted the oceanic circulation, hampered the exchange of water masses and prevented the incursion of radiolarian faunas from the open sea (Fig. 12). The uppermost Sinemurian peak proportion of Saturnalidae (that characteristically abound in enclosed basins with restricted oceanic circulation) could be the first sign of environmental deterioration.
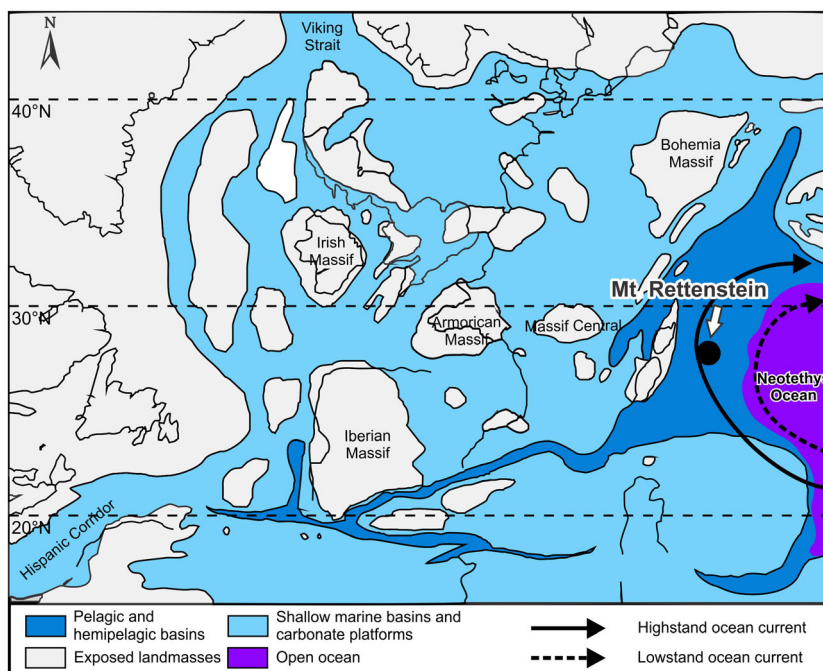
FIG. 12. Late Sinemurian palaeogeographical reconstruction (modified after Thierry 2000), with postulated ocean currents during high and during low sealevels.

The recovery started during the earliest Pliensbachian transgression concomitant with the negative CIE of the S-PBE (Fig. 2). The CIA values from Mount Rettenstein suggest lower precipitation rates in the upper part of the section. The coeval increase in the Sr/Ca ratio indicates a temperature decrease, if we accept that the carbonate was mostly derived from aragonite produced on the adjacent topographic highs. These data are in accordance with the regional oxygen isotope records and elemental geochemical analyses from different locations in the Western Tethyan Realm, demonstrating that during the S-PBE the climate became both colder (e.g. Korte & Hesselbo 2011; Duarte *et al*. 2014; Gómez *et al*. 2016; Price *et al*. 2016; Schöllhorn *et al*. 2020a, 2020b) and drier (Schöllhorn *et al*. 2020b). The reduced continental runoff and thus decreased influx of nutrients would have further reduced the radiolarian productivity and affected the recovery after the late Sinemurian regression. It is worth noting that these drastic changes in the radiolarian assemblages during that time are documented only at Mount Rettenstein, suggesting that the phenomenon was geographically limited. However, beside response of radiolarians studied in this paper, changes (drop in diversity and/or drop in abundance) are also documented for dinoflagellates from the UK and the Iberian Massif (van de Schootbrugge *et al*. 2005) and for benthic foraminifera from the Adriatic Carbonate Platform in Albania (Gawlick & Schlagintweit 2019), thereby leaving open the possibility of geographically more widespread environmental deterioration.

CONCLUSION

The succession of upper Sinemurian to lower Pliensbachian siliceous limestone and marl of Mount Rettenstein was deposited at a water depth of a few hundred metres in a well-oxygenated basin on the western edge of the Neotethys Ocean. The extracted siliceous microfauna is composed of more than 80% sponge spicules and less than 20% radiolarians with a strong predominance of spumellarians. The N/S abundance ratio ranges between 1:5 and 1:3.

A considerable drop in radiolarian diversity occurred at the Sinemurian–Pliensbachian transition and was accompanied by significant changes in relative abundances. The surface-dwelling radiolarians were the most seriously affected. Angulobrachiidae, Hagiastridae, Pantanelliidae (mostly *Gorgansium*), Poulpidae and Ultranaporidae completely or nearly disappeared due to the environmental crisis. The most unaffected genera that survived the crisis and were conspicuously abundant in the aftermath were *Archaeocenosphaera*, *Praeconocaryomma*, *Zhamoidellum* and *Lantus*.

The changes in the taxonomic composition were local and are attributed to a prominent end-Sinemurian

sealevel drop that transformed the area into a semi-enclosed basin with restricted oceanic circulation. The basin was characterized by low radiolarian productivity caused by the weak inflow of fertile waters from the open ocean and a low riverine influx of nutrients due to a cool and arid climate.

Author contributions. **Conceptualization** T Cifer (TC), Š Goričan (ŠG), H-J Gawlick (HJG); **Data Curation** TC; **Funding Acquisition** ŠG, TC, HJG; **Investigation** TC, A Demény (AD); **Project Administration** TC; **Resources** TC, ŠG, AD; **Supervision** ŠG; **Visualization** TC; **Writing – Original Draft preparation** TC; **Writing – Review & Editing** TC, ŠG, HJG, AD.

Editor. Yue Wang

SUPPORTING INFORMATION

Additional Supporting Information can be found online (https://doi.org/10.1002/spp2.1581):

Table S1. Content of measured elements, and values of stable carbon (δ^{13}C) and oxygen (δ^{18}O) isotopes in the analysed samples.

Table S2. Correlation table for the analysed elements and stable carbon and oxygen isotopes.

Table S3. Variations in P [p.p.m.], MnO [%], Ba$_{xs}$ [p.p.m.], and Sr/Ca [mmol/mol] values throughout the studied section.

Table S4. Variations in the chemical index of alteration (CIA) throughout the studied section. CIA was calculated after the formula proposed by Schöllhorn *et al.* (2020b).

Table S5. Stable carbon isotope (δ^{13}C) curve for the studied section.

Table S6. Chart of the origin of silica (SiO_2) in the studied samples (after Barbera *et al.* 2006). All studied samples, except Rö454 and Rö462, have a predominantly biogenic origin of silica.

Table S7. Chart of the pelagic–continental margin origin of siliciclastic components in the samples (after Girty *et al.* 1996).

Table S8. Chart of the origin of the siliciclastic components in the samples (after Boström 1973). The samples plot on the terrigenous line, which excludes a basaltic or hydrothermal origin.

REFERENCES

Auer, M., Gawlick, H.-J., Suzuki, H. and Schlagintweit, F. 2009. Spatial and temporal development of siliceous basin and shallow-water carbonate sedimentation in Oxfordian Northern Calcareous Alps. *Facies*, **55**, 63–87.

Barbera, G., Mazzoleni, P., Critelli, S., Pappalardo, A., Lo Giudice, A. and Cirrincione, R. 2006. Provenance of shales and sedimentary history of the Monte Soro Unit, Sicily. *Periodico di Mineralogia*, **75**, 313–330.

Bartolini, A., Baumgartner, P. O. and Guex, J. 1999. Middle and Late Jurassic radiolarian palaeoecology versus carbon-isotope stratigraphy. *Palaeogeography, Palaeoclimatology, Palaeoecology*, **145**, 43–60.

Baumgartner, P. O. 1987. Age and genesis of Tethyan Jurassic radiolarites. *Eclogae Geologicae Helvetiae*, **80**, 831–879.

Baumgartner, P. O. 1993. Early Cretaceous radiolarians of the Northeast Indian Ocean (Leg 123: Sites 765, 766 and DSDP Site 261): the Antarctic–Tethys connection. *Marine Micropaleontology*, **21**, 329–352.

Baumgartner, P. O., Bown, P., Marcoux, J., Mutterlose, J., Kaminski, M., Haig, D. and McMinn, A. 1992. Early Cretaceous biogeographic and oceanographic synthesis of Leg 123 (off Northwestern Australia). *Proceedings of the Ocean Drilling Program, Scientific Results*, **123**, 739–758.

Baumgartner, P. O., Li, X., Matsuoka, A. and Vérard, C. 2023. Austral and subtropical gyre Radiolaria: latest Jurassic to early Cretaceous Leg 123, Site 765, Argo Abyssal Plain revisited: southern hemisphere paleobiogeography and global climate change. *Micropaleontology*, **69**, 555–633.

Blome, C. D. 1987. Paleogeographic significance of lower Mesozoic radiolarians from the Brooks Range, Alaska. 371–380. *In* Tailleur, I. and Weimer, P. (eds) *Alaskan North Slope geology*. Pacific Section, Society of Economic Paleontologists & Mineralogists.

Böhm, F. 2003. Lithostratigraphy of the Adnet Group (Lower to Middle Jurassic, Salzburg, Austria). 231–268. *In* Piller, W. E. (ed.) *Stratigraphia Austriaca*. Österreichische Akademie der Wissenschaften, Schriftenreihe der Erdwissenschaftlichen Kommissionen **16**.

Boltovskoy, D. 2017. Vertical distribution patterns of Radiolaria Polycystina (Protista) in the World Ocean: living ranges, isothermal submersion and settling shells. *Journal of Plankton Research*, **39**, 330–349.

Boltovskoy, D. and Correa, N. 2017. Planktonic equatorial diversity troughs: fact or artifact? Latitudinal diversity gradients in Radiolaria. *Ecology*, **98**, 112–124.

Boltovskoy, D., Kling, S. A., Takahashi, K. and Bjørklund, K. 2010. World atlas of distribution of Recent Polycystina (Radiolaria). *Palaeontologia Electronica*, **13** (3), 18A, 230 pp.

Boltovskoy, D., Anderson, O. R. and Correa, N. M. 2017. Radiolaria and Phaeodaria. 731–763. *In* Archibald, J. M., Simpson, A. G. B. and Slamovits, C. H. (eds) *Handbook of the protists*. Springer International Publishing.

Boström, K. 1973. The origin and fate of ferromanganoan active ridge sediments. *Stockholm Contributions in Geology*, **27**, 147–243.

Carter, E. S. and Haggart, J. W. 2006. Radiolarian biogeography of the Pacific region indicates a mid- to high-latitude (30°) position for the Insular superterrane since the late Early Jurassic. 109–131. *In* Haggart, J. W., Enkin, R. J. and Monger, J. W. H. (eds) *Paleogeography of the North American Cordillera:*

Evidence for and against large-scale displacements. Geological Association of Canada, Special Paper, **46**.

Carter, E. S., Goričan, Š., Guex, J., O'Dogherty, L., De Wever, P., Dumitrica, P., Hori, R. S., Matsuoka, A. and Whalen, P. A. 2010. Global radiolarian zonation for the Pliensbachian, Toarcian and Aalenian. *Palaeogeography, Palaeoclimatology, Palaeoecology*, **297**, 401–419.

Casacci, M., Bertinelli, A., Algeo, T. J. and Rigo, M. 2016. Carbonate-to-biosilica transition at the Norian–Rhaetian boundary controlled by rift-related subsidence in the western Tethyan Lagonegro Basin (southern Italy). *Palaeogeography, Palaeoclimatology, Palaeoecology*, **456**, 21–36.

Casey, R. E. 1977. The ecology and distribution of Recent Radiolaria. 809–838. *In* Ramsay, A. T. S. (ed.) *Oceanic micropalaeontology*. Academic Press.

Casey, R. E. 1979. Model of modern Polycystine radiolarian shallow-water zoogeography. *Palaeogeography, Palaeoclimatology, Palaeoecology*, **74**, 15–22.

Casey, R. E. 1987. Radiolaria–241. *In* Broadhead, T. W. (ed.) *Fossil prokaryotes and protists: Notes for a short course*. University of Tennessee, Department of Geological Sciences, 213, Studies in Geology **18**.

Cifer, T. and Goričan, Š. 2023a. Late Sinemurian and early Pliensbachian Radiolaria from Mount Rettenstein (Northern Calcareous Alps, Austria). Part 1. Nassellaria. *Revue de Micropaléontologie*, **79**, 100717.

Cifer, T. and Goričan, Š. 2023b. Late Sinemurian and early Pliensbachian Radiolaria from Mount Rettenstein (Northern Calcareous Alps, Austria). Part 2. Entactinaria and Spumellaria. *Revue de Micropaléontologie*, **81**, 100752.

Cifer, T., Goričan, Š., Gawlick, H.-J. and Auer, M. 2020. Pliensbachian, Early Jurassic radiolarians from Mount Rettenstein in the Northern Calcareous Alps, Austria. *Acta Palaeontologica Polonica*, **65**, 167–207.

Cifer, T., Goričan, Š., Auer, M., Demény, A., Fraguas, Á., Gawlick, H.-J. and Riechelmann, S. 2022. Integrated stratigraphy (radiolarians, calcareous nannofossils, carbon and strontium isotopes) of the Sinemurian–Pliensbachian transition at Mt. Rettenstein, Northern calcareous Alps, Austria. *Global & Planetary Change*, **212**, 103811.

Danisch, J., Kabiri, L., Nutz, A. and Bodin, S. 2019. Chemostratigraphy of Late Sinemurian-Early Pliensbachian shallow-to deep-water deposits of the Central High Atlas Basin: paleoenvironmental implications. *Journal of African Earth Sciences*, **153**, 239–249.

Duarte, L. V., Comas-Rengifo, M. J., Silva, R. L., Paredes, R. and Goy, A. 2014. Carbon isotope stratigraphy and ammonite biochronostratigraphy across the Sinemurian–Pliensbachian boundary in the western Iberian margin. *Bulletin of Geosciences*, **89**, 719–736.

Empson-Morin, K. M. 1984. Depth and latitude distribution of Radiolaria in Campanian (Late Cretaceous) tropical and subtropical oceans. *Micropaleontology*, **30**, 87–115.

Flügel, E. 2004. *Microfacies of carbonate rocks: Analysis, interpretation and application*. Springer, 978 pp.

Franceschi, M., Dal Corso, J., Posenato, R., Roghi, G., Masetti, D. and Jenkyns, H. C. 2014. Early Pliensbachian (Early Jurassic) C-isotope perturbation and the diffusion of the Lithiotis Fauna: insights from the western Tethys. *Palaeogeography, Palaeoclimatology, Palaeoecology*, **410**, 255–263.

Franceschi, M., Dal Corso, J., Cobianchi, M., Roghi, G., Penasa, L., Picotti, V. and Preto, N. 2019. Tethyan carbonate platform transformations during the Early Jurassic (Sinemurian–Pliensbachian, Southern Alps): comparison with the Late Triassic Carnian Pluvial Episode. *Bulletin of the Geological Society of America*, **131**, 1255–1275.

Frisch, W. and Gawlick, H.-J. 2003. The nappe structure of the central Northern Calcareous Alps and its disintegration during Miocene tectonic extrusion: a contribution to understanding the orogenic evolution of the Eastern Alps. *International Journal of Earth Sciences*, **92**, 712–727.

Gawlick, H.-J. and Missoni, S. 2019. Middle–Late Jurassic sedimentary mélange formation related to ophiolite obduction in the Alpine-Carpathian-Dinaridic Mountain Range. *Gondwana Research*, **74**, 144–172.

Gawlick, H.-J. and Schlagintweit, F. 2019. Triassic to Lower Jurassic shallow-water carbonates north of Lake Shkodra (NW Albania, Albanian Alps Zone): part of the Adriatic Carbonate Platform basement. *Acta Palaeontologica Romaniae*, **15**, 3–12.

Gawlick, H.-J., Missoni, S., Schlagintweit, F., Suzuki, H., Frisch, W., Krystyn, L., Blau, J. and Lein, R. 2009. Jurassic tectonostratigraphy of the Austroalpine domain. *Mitteilungen der Gesellschaft der Geologie- und Bergbaustudenten in Österreich*, **50**, 1–152.

Girty, G. H., Ridge, D. L., Knaack, C., Johnson, D. and Al-Riyami, R. K. 1996. Provenance and depositional setting of Paleozoic chert and argillite, Sierra Nevada, California. *Journal of Sedimentary Research*, **66**, 107–118.

Gómez, J. J., Comas-Rengifo, M. J. and Goy, A. 2016. Palaeoclimatic oscillations in the Pliensbachian (Early Jurassic) of the Asturian Basin (Northern Spain). *Climate of the Past*, **12**, 1199–1214.

Goričan, Š., Šmuc, A. and Baumgartner, P. O. 2003. Toarcian Radiolaria from Mt. Mangart (Slovenian–Italian border) and their paleoecological implications. *Marine Micropaleontology*, **49**, 275–301.

Halamić, J., Marchig, V. and Goričan, Š. 2005. Jurassic radiolarian cherts in north-western Croatia: geochemistry, material provenance and depositional environment. *Geologica Carpathica*, **56**, 123–136.

Hallam, A. 1988. A reevaluation of Jurassic eustasy in the light of new data and the revised Exxon curve. 261–273. *In* Wilgus, C. K., Hastings, B. S., Ross, C. A., Posamentier, H., Van Wagoner, J. and Kendall, C. G. S. C. (eds) *Sea level changes: An integrated approach*. SEPM Special Publication, **42**.

Haq, B. U. 2018. Jurassic sea-level variations: a reappraisal. *GSA Today*, **28**, 4–10.

Hesselbo, S. P. and Jenkyns, H. C. 1998. British Lower Jurassic sequence stratigraphy. 561–581. *In* De Graciansky, P.-C., Hardenbol, J., Jacquin, T. and Vail, P. R. (eds) *Mesozoic and Cenozoic sequence stratigraphy of European basins*. SEPM Special Publication, **60**.

Hesselbo, S. P., Meister, C. and Gröcke, D. R. 2000. A potential global stratotype for the Sinemurian–Pliensbachian boundary (Lower Jurassic), Robin Hood's Bay, UK: ammonite faunas and isotope stratigraphy. *Geological Magazine*, **137**, 601–607.

Hori, R. S. 1993. Pantanelliidae abundance for lower Jurassic siliceous rocks. *News of Osaka Micropaleontologists*, **9**, 101–108.

Hori, R. S., Cho, C.-F. and Umeda, H. 1993. Origin of cyclicity in Triassic–Jurassic radiolarian bedded cherts of the Mino accretionary complex from Japan. *Island Arc*, **3**, 170–180.

Hull, D. M. 1995. Morphologic diversity and paleogeographic significance of the Family Parvicingulidae (Radiolaria). *Micropaleontology*, **41**, 1–48.

Jenkyns, H. C. 2020. The demise and drowning of Early Jurassic (Sinemurian) carbonate platforms: stratigraphic evidence from the Italian peninsula, Sicily and Spain. 55–82. *In* Catalano, R., Barberi, F., Bernoulli, D., D'Argenio, B., Dal Piaz, G. V., Doglioni, C., Panza, G. F. and Praturlon, A. (eds) *L'Eredità scientifica di Paolo Scandone, geologo*. Accademia Nazionale de Lincei, Atti dei Convegni Lincei, **355**.

Jenkyns, H. C. and Weedon, G. P. 2013. Chemostratigraphy (CaCO$_3$, Toc, $\delta^{13}C_{org}$) of Sinemurian (Lower Jurassic) black shales from the Wessex Basin, Dorset and palaeoenvironmental implications. *Newsletters on Stratigraphy*, **46**, 1–21.

Jenkyns, H. C., Jones, C. E., Gröcke, D. R., Hesselbo, S. P. and Parkinson, D. N. 2002. Chemostratigraphy of the Jurassic System: applications, limitations and implications for palaeoceanography. *Journal of the Geological Society, London*, **159**, 351–378.

Karamata, S. 2006. The geological development of the Balkan Peninsula related to the approach, collision and compression of Gondwanan and Eurasian units. 155–178. *In* Robertson, A. H. F. and Mountrakis, D. (eds) *Tectonic development of the Eastern Mediterranean Region*. Geological Society, London, Special Publications, **260**.

Kiessling, W. 1996. Facies characterization of mid-Mesozoic deep-water sediments by quantitative analysis of siliceous microfaunas. *Facies*, **35**, 237–274.

Kiessling, W. 1999. Late Jurassic radiolarians from the Antarctic Peninsula. *Micropalaeontology*, **45**, 1–96.

Korte, C. and Hesselbo, S. P. 2011. Shallow marine carbon and oxygen isotope and elemental records indicate icehouse-greenhouse cycles during the Early Jurassic. *Paleoceanography*, **26**, PA4219.

Landis, G. P. 1983. Harding Iceland Spar: a new $\delta^{18}O$-$\delta^{13}C$ carbonate standard for hydrothermal minerals. *Chemical Geology*, **41**, 91–94.

Mattioli, E. and Pittet, B. 2002. Contribution of calcareous nannoplankton to carbonate deposition: a new approach applied to the Lower Jurassic of central Italy. *Marine Micropaleontology*, **45**, 175–190.

McMillen, K. J. and Casey, R. E. 1978. Distribution of living polycystine radiolarians in the Gulf of Mexico and Caribbean Sea, and comparison with the sedimentary record. *Marine Micropaleontology*, **3**, 121–145.

Meister, C. and Böhm, F. 1993. Austroalpine Liassic Ammonites from the Adnet Formation (Northern Calcareous Alps). *Jahrbuch der Geologischen Bundesanstalt*, **136**, 163–211.

Mekik, F. 2000. Early Cretaceous Pantanelliidae (Radiolaria) from northwest Turkey. *Micropaleontology*, **46**, 1–30.

Mercuzot, M., Pellenard, P., Durlet, C., Bougeault, C., Meister, C., Dommergues, J.-L., Thibault, N., Baudin, F., Mathieu, O.,

Bruneau, L., Huret, E. and El Hmidi, K. 2020. Carbon-isotope events during the Pliensbachian (Lower Jurassic) on the African and European margins of the NW Tethyan Realm. *Newsletters on Stratigraphy*, **53**, 41–69.

Murchey, B. L. 1990. Age and depositional setting of siliceous sediments in the upper Paleozoic Havallah sequence near Battle Mountain, Nevada; implications for the paleogeography and structural evolution of the western margin of North America. 137–155. *In* Harwood, D. S. and Miller, M. M. (eds) *Paleozoic and early Mesozoic paleogeographic relations; Sierra Nevada, Klamath Mountains, and related terranes*. Geological Society of America, Special Paper **255**.

Murchey, B. L. 2004. Regional analysis of spiculite faunas in the Permian Phosphoria Basin: implications for paleoceanography. 111–135. *In* Hein, J. R. (ed.) *Life cycle of the Phosphoria Formation: From deposition to the post-mining environment*. Elsevier, Handbook of Exploration Geochemistry, **8**.

Musavu-Moussavou, B., Danelian, T., Baudin, F., Coccioni, R. and Frohlich, F. 2007. The Radiolarian biotic during OAE2. A high-resolution study across the Bonarelli level at Bottaccione (Gubbio, Italy). *Revue de Micropaléontologie*, **50**, 253–287.

O'Dogherty, L., Carter, E. S., Dumitrica, P., Goričan, Š., De Wever, P., Hungerbühler, A., Bandini, A. N. and Takemura, A. 2009. Catalogue of Mesozoic radiolarian genera: Part 2, Jurassic–Cretaceous. *Geodiversitas*, **31**, 271–356.

Oliveira, L. C., Rodrigues, R., Duarte, L. V. and Lemos, V. B. 2006. Avaliação do potencial gerador de petróleo e interpretação paleoambiental com base em biomarca-dores e isótopos estáveis de carbono da seção Pliensba-quiano – Toarciano inferior (Jurássico Inferior) da região de Peniche (Bacia Lusitânica, Portugal). *Boletim de Geociências da Petrobras*, **14**, 207–234.

Pessagno, E. A. Jr and Blome, C. D. 1986. Faunal affinities and tectogenesis of Mesozoic rocks in the Blue Mountain Province of eastern Oregon and western Idaho. 65–78. *In* Vallier, T. L. and Brooks, H. C. (eds) *Geology of the Blue Mountains region of Oregon, Idaho and Washington: Biostratigraphy and paleontology*. US Geological Survey Professional Papers **1435**.

Peti, L. and Thibault, N. 2022. Early Jurassic coccolith diversification and response to pre-Toarcian environmental changes: a perspective from the Paris Basin. *Marine Micropaleontology*, **177**, 102173.

Peti, L., Thibault, N., Clémence, M.-E., Korte, C., Dommergues, J.-L., Bougeault, C., Pellenard, P., Jelby, M. E. and Ullmann, C. V. 2017. Sinemurian–Pliensbachian calcareous nannofossil biostratigraphy and organic carbon isotope stratigraphy in the Paris Basin: calibration to the ammonite biozonation of NW Europe. *Palaeogeography, Palaeoclimatology, Palaeoecology*, **468**, 142–161.

Price, G. D., Baker, S. J., Van De Velde, J. and Clémence, M.-E. 2016. High-resolution carbon cycle and seawater temperature evolution during the Early Jurassic (Sinemurian-Early Pliensbachian). *Geochemistry, Geophysics, Geosystems*, **17**, 3917–3928.

Rosales, I., Quesada, S. and Robles, S. 2001. Primary and diagenetic isotopic signals in fossils and hemipelagic carbonates: the Lower Jurassic of northern Spain. *Sedimentology*, **48**, 1149–1169.

Rosales, I., Quesada, S. and Robles, S. 2004. Paleotemperature variations of Early Jurassic seawater recorded in geochemical

trends of belemnites from the Basque–Cantabrian basin, northern Spain. *Palaeogeography, Palaeoclimatology, Palaeoecology*, **203**, 253–275.

Ruhl, M., Hesselbo, S. P., Hinnov, L., Jenkyns, H. C., Xu, W., Riding, J. B., Storm, M., Minisini, D., Ullmann, C. V. and Leng, M. J. 2016. Astronomical constraints on the duration of the Early Jurassic Pliensbachian Stage and global climatic fluctuations. *Earth & Planetary Science Letters*, **455**, 149–165.

Schoepfer, S. D., Shen, J., Hengye, W., Tyson, R. V., Ingall, E. and Algeo, T. J. 2015. Total organic carbon, organic phosphorus, and biogenic barium fluxes as proxies for paleomarine productivity. *Earth-Science Reviews*, **149**, 23–52.

Schöllhorn, I., Adatte, T., Charbonnier, G., Mattioli, E., Spangenberg, J. E. and Föllmi, K. B. 2020a. Pliensbachian environmental perturbations and their potential link with volcanic activity: Swiss and British geochemical records. *Sedimentary Geology*, **406**, 105665.

Schöllhorn, I., Adatte, T., van de Schootbrugge, B., Houben, A., Charbonnier, G., Janssen, N. and Föllmi, K. B. 2020b. Climate and environmental response to the break-up of Pangea during the Early Jurassic (Hettangian-Pliensbachian);

the Dorset coast (UK) revisited. *Global & Planetary Change*, **185**, 103096.

Scotese, C. R. 2002. PALEOMAP website. http://scotese.com

Storm, M. S., Hesselbo, S. P., Jenkyns, H. C., Ruhl, M., Ullmann, C. V., Xu, W., Leng, M. J., Riding, J. B. and Gorbanenko, O. 2020. Orbital pacing and secular evolution of the Early Jurassic carbon cycle. *Proceedings of the National Academy of Sciences*, **117**, 3974–3982.

Thierry, J. 2000. Late Sinemurian (193–191 Ma). 49–59. *In* Dercourt, J., Gaetani, M., Vrielynck, B., Barrier, E., Biju-Duval, B., Brunet, M.-F., Cadet, J.-P., Crasquin, S. and Sandulescu, M. (eds) *Atlas Peri-Tethys, palaeogeographical maps*. Commission del la Carte Géologique du Monde, Paris.

van de Schootbrugge, B., Bailey, T. R., Rosenthal, Y., Katz, M. E., Wright, J. D., Miller, K. G., Feist-Burkhardt, S. and Falkowski, P. G. 2005. Early Jurassic climate change and the radiation of organic-walled phytoplankton in the Tethys Ocean. *Paleobiology*, **31**, 73–97.

Zügel, P., Riegraf, W., Schweigert, G. and Dietl, G. 1998. Radiolaria from the Nusplingen Lithographic Limestone (Late Kimmeridgian, SW Germany). *Stuttgarter Beiträge zur Naturkunde, B*, **268**, 1–43.